Cell Reports

Article

GDE2-Dependent Activation of Canonical Wnt Signaling in Neurons Regulates Oligodendrocyte Maturation

Graphical Abstract

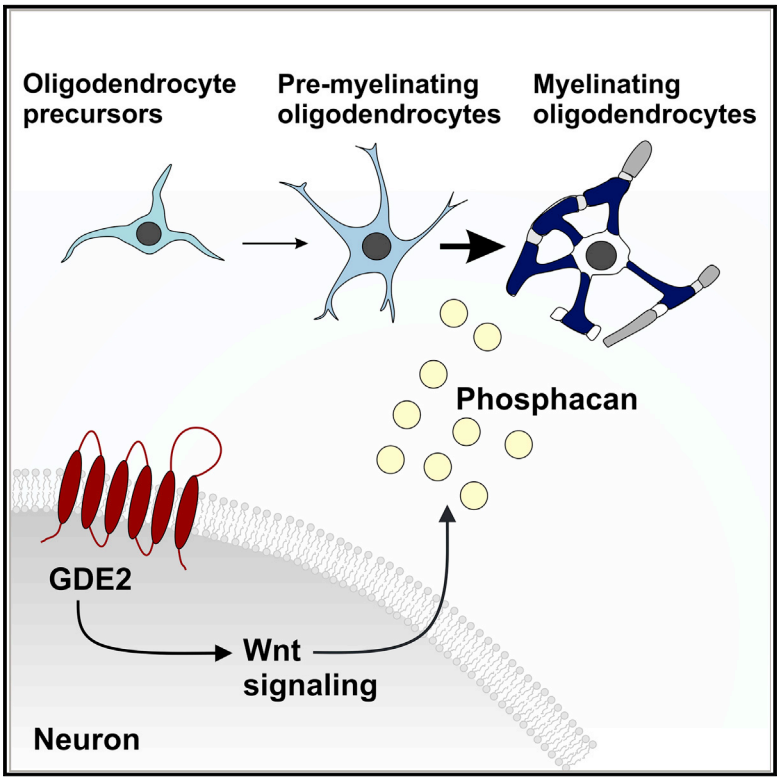

Authors

Bo-Ran Choi, Clinton Cave, Chan Hyun Na, Shanthini Sockanathan

Correspondence

ssockan1@jhmi.edu

In Brief

Communication between neurons and oligodendroglial cells regulates oligodendrocyte development. Here, Choi et al. show that the six-transmembrane GPI-anchor-cleaving enzyme GDE2 stimulates canonical Wnt signaling in neurons to release soluble factors, such as phosphacan, to promote oligodendrocyte maturation.

Highlights

- GDE2 is expressed in neurons and a subset of oligodendrocytes
- Loss of neuronal GDE2 delays oligodendrocyte maturation and impairs myelination
- GDE2 stimulates canonical Wnt signaling in neurons, which releases phosphacan
- Neuronally derived phosphacan promotes oligodendrocyte maturation

Choi et al., 2020, Cell Reports *31*, 107540
May 5, 2020
https://doi.org/10.1016/j.celrep.2020.107540

CellPress

Cell Reports

CellPress
OPEN ACCESS

Article

GDE2-Dependent Activation of Canonical Wnt Signaling in Neurons Regulates Oligodendrocyte Maturation

Bo-Ran Choi,[1] Clinton Cave,[2] Chan Hyun Na,[3] and Shanthini Sockanathan[1,4,*]

[1]The Solomon H. Snyder Department of Neuroscience, Johns Hopkins University School of Medicine, 725 N. Wolfe Street, PCTB 1004, Baltimore, MD 21205, USA

[2]Neuroscience Program, Middlebury College, 276 Bicentennial Way, MBH 351, Middlebury, VT 05753, USA

[3]Department of Neurology, Institute for Cell Engineering, Johns Hopkins University School of Medicine, 733 N. Broadway, MRB 753, Baltimore, MD 21205, USA

[4]Lead Contact

*Correspondence: ssockan1@jhmi.edu

https://doi.org/10.1016/j.celrep.2020.107540

SUMMARY

Neurons and oligodendrocytes communicate to regulate oligodendrocyte development and ensure appropriate axonal myelination. Here, we show that Glycerophosphodiester phosphodiesterase 2 (GDE2) signaling underlies a neuronal pathway that promotes oligodendrocyte maturation through the release of soluble neuronally derived factors. Mice lacking global or neuronal GDE2 expression have reduced mature oligodendrocytes and myelin proteins but retain normal numbers of oligodendrocyte precursor cells (OPCs). Wild-type (WT) OPCs cultured in conditioned medium (CM) from *Gde2*-null (*Gde2KO*) neurons exhibit delayed maturation, recapitulating *in vivo* phenotypes. *Gde2KO* neurons show robust reduction in canonical Wnt signaling, and genetic activation of Wnt signaling in *Gde2KO* neurons rescues *in vivo* and *in vitro* oligodendrocyte maturation. Phosphacan, a known stimulant of oligodendrocyte maturation, is reduced in CM from *Gde2KO* neurons but is restored when Wnt signaling is activated. These studies identify GDE2 control of Wnt signaling as a neuronal pathway that signals to oligodendroglia to promote oligodendrocyte maturation.

INTRODUCTION

Oligodendrocytes (OLs) are important regulators of neural circuit function. OLs produce myelin, a lipid-rich extension of their plasma membrane that wraps axons and facilitates the fast, saltatory conduction of action potentials. In addition, OLs serve as a source of metabolic support for neurons that help promote neuronal health and survival (Nave, 2010). The remarkable match between the number of myelinating OLs and axons that require myelination (Davison and Peters, 1970) suggests that communication between axons and OL lineage cells is involved in coordinating OL proliferation, survival, and maturation. However, neuronal pathways that control the timing of OL maturation are not well understood.

OLs in the brain are generated from three major waves of OL precursor cell (OPC) production that originate first subcortically and then cortically (Kessaris et al., 2006). OPCs exhibit regional diversity in terms of their proliferative, migratory, and remyelination properties (Lentferink et al., 2018; Power et al., 2002; Spitzer et al., 2019). However, genetic ablation studies indicate that ventrally and dorsally derived OPC populations are functionally redundant (Kessaris et al., 2006); thus, the physiological basis of OPC diversity remains unclear. OPCs cultured *in vitro* can proliferate and differentiate into myelinating OLs in the absence of neurons (Barres et al., 1993); nevertheless, neurons *in vivo* appear to play important roles in coordinating multiple aspects of OL development. Nerve transection or silencing of neuronal activity shows profound loss of OPC proliferation, survival, and myelination (Barres and Raff, 1993; Ueda et al., 1999), and roles for experience, learning, and environmental factors are emerging as important contributors to myelination in development and in adulthood (Gibson et al., 2014; Makinodan et al., 2012; Mayoral and Chan, 2016).

What are the mechanisms by which neurons regulate OL differentiation and myelination? OPCs that make stable contact with axons differentiate into myelinating OLs, and this is mediated by surface-localized receptors and adhesion molecules that converge to stimulate activity of the non-receptor Src-family tyrosine kinase Fyn in OPCs (Umemori et al., 1994). Interestingly, many contact-mediated cues appear to inhibit OL differentiation, presumably to ensure the appropriate timing of axonal myelination during development. For example, polysialylated neuronal cell adhesion molecule (PSA-NCAM) inhibits OPC differentiation and is downregulated to coincide with myelination (Charles et al., 2000), as is the canonical Notch ligand Jagged, which is expressed on axons and binds the Notch receptor on OPCs to inhibit OL differentiation (Wang et al., 1998). The finding that OLs cultured with inert polystyrene fibers exhibit a size-dependent ensheathment of 0.4 μm fibers or more suggests that axonal caliber also contributes to OL

myelination (Lee et al., 2012). Of note, both myelinated and unmyelinated axons range in diameter from 0.2 to 0.8 μm *in vivo* (Remahl and Hildebrand, 1982), suggesting the existence of repulsive and instructive axonal cues that integrate axonal caliber with OL developmental mechanisms. One such cue is likely to involve Akt-mTOR signaling, as activation of this pathway increases the caliber of normally unmyelinated cerebellar axons and expands OPC progenitors and production of myelinating OLs (Goebbels et al., 2016). Another major factor that influences OL proliferation, differentiation, and maturation is neuronal activity. Neuronal activity releases adenosine and glutamate, which regulates the proliferation and differentiation of OPCs into myelinating OLs (Stevens et al., 2002; Yuan et al., 1998). ATP released by electrically active neurons can stimulate astrocytes to produce leukemia inhibitory factor (LIF), which promotes OL differentiation (Ishibashi et al., 2006). Thus, contact-mediated signals, axon caliber, and neuronal activity are important for OL development. Other neuronally derived pathways that regulate OL differentiation and maturation are not well defined.

Glycerophosphodiester phosphodiesterase 2 (GDE2 or GDPD5) is a six-transmembrane protein that contains an external enzymatic domain that is homologous to bacterial glycerophosphodiester phosphodiesterases (GDPDs) (Rao and Sockanathan, 2005). GDE2 and its family members GDE3 and GDE6 are the only known enzymes in vertebrates that regulate the function of glycosylphosphatidylinositol (GPI)-anchored proteins on the plasma membrane through cleavage at the GPI-anchor (Park et al., 2013). During embryonic development, GDE2 regulates the timing of cortical and spinal motor neuron differentiation to promote late-born neuronal subtypes by downregulating Notch signaling (Rodriguez et al., 2012). In developing spinal motor neurons, GDE2 downregulates Notch activation by releasing the GPI-anchored Notch activator reversion-inducing cysteine-rich protein with Kazal motifs (RECK) from motor neuron surfaces (Park et al., 2013). GDE2 GPI-anchor cleavage activity is also implicated in promoting neuroblastoma differentiation, in this case through release of the heparan sulfate proteoglycan GPC6 (Matas-Rico et al., 2016). In addition, GDE2 is required for motor neuron survival, and genetic studies indicate that these functions are distinct from its role in embryonic development (Cave et al., 2017).

We show here that GDE2 functions in neurons to regulate the timing of OL development. GDE2 is required to maintain canonical Wnt signaling in neurons, and this pathway is responsible for the release of soluble factors such as phosphacan that promote OL maturation. These studies identify a neuronal mechanism that controls OL differentiation and maturation and reveals roles for soluble, neuronally derived factors in regulating the production of myelinating OLs.

RESULTS

Gde2 Is Primarily Expressed in Neurons in the Postnatal Brain

Fluorescence *in situ* hybridization (FISH) detects *Gde2* transcripts in the hippocampus, thalamus, caudoputamen, cortex (CTX), and medial habenula at postnatal day 11 (P11) mouse brain (Figure 1A). *Gde2* mRNA is initially expressed in deep cortical layers V and VI but expands to upper cortical layers at later stages (Figures 1B, 1C, and S1C). Western blot confirms GDE2 protein expression in postnatal cortices, with increasing GDE2 expression from P7 to P14 and continued expression at 1 and 2 months of age (Figures S1A–S1C). FISH combined with immunohistochemical detection of neuronal (NeuN) markers detects *Gde2* transcript expression in neurons at P11 with ~98% of NeuN$^+$ neurons expressing *Gde2* mRNA (Figures 1B and 1D). Western blot of protein extracts from cultured cortical neurons confirms neuronal expression of GDE2 protein (Figure S1D). *Gde2* transcripts are also detected in ~20% of Olig2$^+$ oligodendroglial cells, but levels of *Gde2* transcript expression in Olig2$^+$ cells are markedly lower than in neurons (Figure 1B and 1D). Quantitative PCR (qPCR) from cultured OPCs isolated from P6 cortices reveal minimal *Gde2* expression in proliferating OPCs; however, differentiated OLs express both *Gde2* transcripts and GDE2 protein (Figures S1E and S1F). Thus, *Gde2* is predominantly expressed in neurons during early postnatal development, with lower levels of expression in a subset of OLs.

GDE2 Ablation Delays OL Maturation

Mice genetically ablated for GDE2 (*Gde2KO*) show delayed production of deep-layer neurons and increased production of superficial cortical neurons during embryonic development (Rodriguez et al., 2012). We examined *Gde2KO* animals at P11–P15 when neuronal migration is complete and detected no discernible differences in cortical lamination, neuronal numbers, or morphology in *Gde2KO* animals compared with wild-type (WT) littermates, suggesting that early perturbations in neurogenesis have normalized by this time point (Figure S2A). The period of increased GDE2 expression in mouse CTX (P7–P14; Figure S1A) coincides with the period of OL differentiation and maturation (Trapp et al., 1997). Further, the spatiotemporal expression of GDE2 correlates with the pattern of cortical OL maturation and myelination, which initiates in deep cortical layers and extends to superficial laminae (Tomassy et al., 2014) (Figures 1A–1C). To determine if GDE2 regulates OL maturation, we examined OL development in *Gde2KO* animals at P7 and at P11, focusing specifically on the corpus callosum (CC) and adjacent motor and retrosplenial CTX. OPCs that are actively proliferating are identified by coexpression of the OL lineage determinants Olig2 and Sox10 and the proliferation marker Ki67 (Kuhlbrodt et al., 1998; Zhou et al., 2000) (Figures S2B and S2C). Quantification of Ki67/SOX10/Olig2$^+$ OPCs showed equivalent numbers of proliferating OPCs in WT and *Gde2KO* CC and CTX at P7, suggesting that loss of GDE2 does not affect OPC production (Figure S2D). OPCs stop dividing and differentiate into premyelinating and myelinating OLs, which express CC1, and myelin basic protein (*Mbp*) transcripts (Bhat et al., 1996; Dugas et al., 2006) (Figure S2B). At P11, overall numbers of OL lineage cells (Olig2$^+$) in CC and CTX were equivalent between *Gde2KO* animals and WT controls (Figure 2A and 2B). However, *Gde2KO* animals exhibited a 30% reduction of Olig2$^+$ CC1$^+$ cells and decreased *Mbp* expression in CC and CTX compared with WT (Figure 2A and 2B). Further, cells that

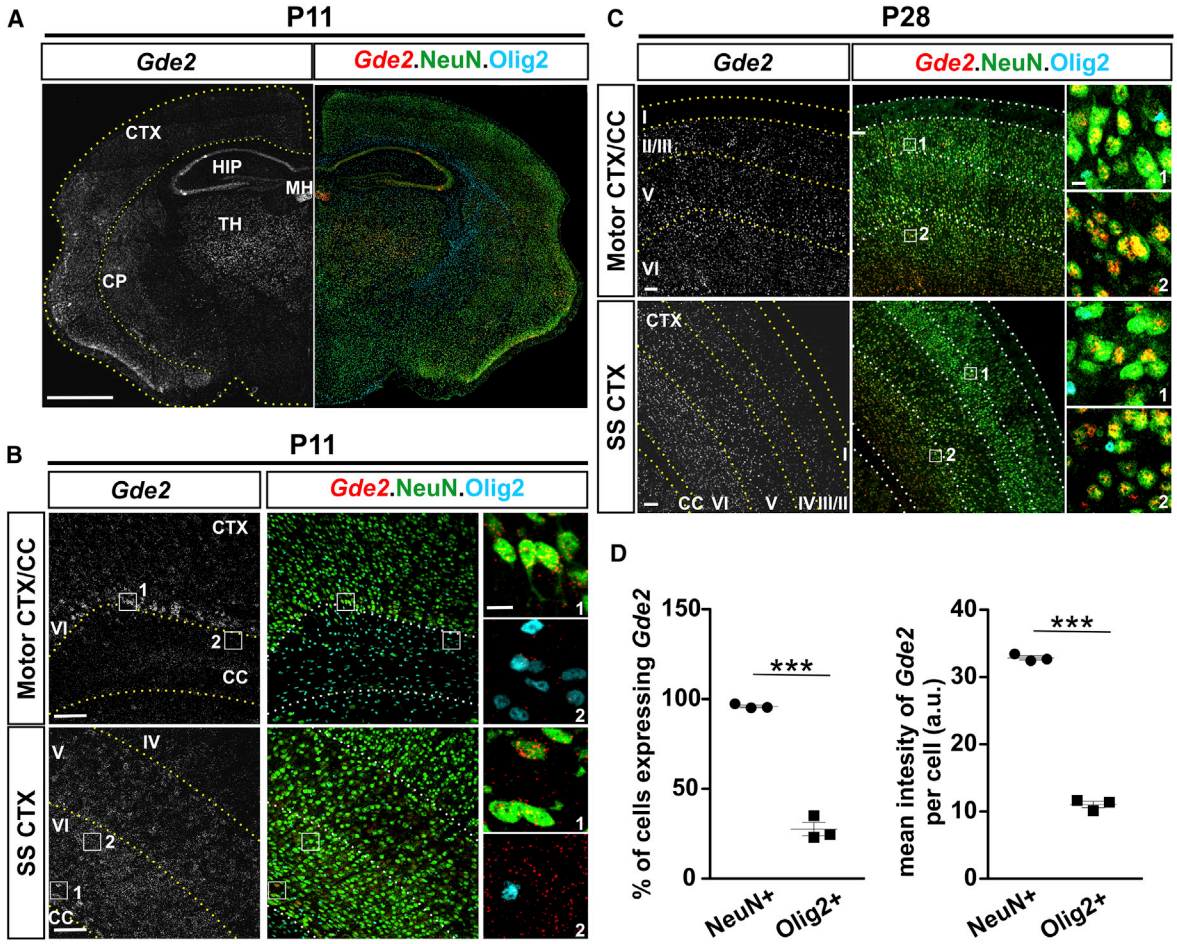

Figure 1. *Gde2* Is Expressed in Neurons and Oligodendrocytes (OLs) in Postnatal Brain

(A–C) FISH of *Gde2* mRNA in coronal cortical sections in different brain areas and postnatal stages. CTX, cortex; SS, somatosensory; CC, corpus callosum; HIP, hippocampus; TH, thalamus; CP, caudoputamen; MH, medial habenula. Hatched lines mark cortical layers. Boxes 1 and 2 in (B) and (C) are magnified in the corresponding panels.

(D) Graphs quantifying *Gde2* mRNA expression. a.u., arbitrary units. ***$p < 0.0001$. n = 3 WT, n = 3 *Gde2KO*. Data are presented as mean ± SEM; two-tailed unpaired Student's t test.

Scale bars represent 1,000 μm (A), 100 μm (B and C), and 10 μm (insets, B and C).

expressed *Mbp* in *Gde2KO* animals had consistently less elaborations than their WT counterparts (Figure 2A). The number of $CC1^+$ cells in *Gde2KO* cortices was reduced in rostral, medial, and caudal regions, indicating a requirement for GDE2 in $CC1^+$ OL generation across the rostral-caudal axis (Figure S2G). Notably, no changes in the number of immature, newly differentiating OLs ($TCF4^+/CC1^-$) were found between WT and *Gde2KO* brain at these stages (Figures S2E and S2F). These observations suggest that GDE2 is not required for the generation or initiation of OPC differentiation but is instead required for OL maturation. In support of this notion, the number of mature myelinating OLs, identified by expression of aspartocylase (ASPA) protein (Madhavarao et al., 2004), was markedly reduced in P15 *Gde2KO* mice compared with WT littermates (Figures S3A and S3B). Further, western blot of P14 cortical extracts revealed robust reduction of myelin proteins MBP and myelin OL glycoprotein (MOG) (Solly et al., 1996) in *Gde2KO* condition but equivalent levels of Olig2 and platelet-derived growth factor receptor alpha (PDGFRα) (Figures 2C and 2D).

Electron microscopy (EM) of P14 cortices showed that *Gde2KO* animals had fewer numbers of myelinated axons compared with WT at P14 (Figures 2E and 2F). Notably, axons that were myelinated had increased g-ratio (ratio of axonal diameter to outer diameter) indicative of hypomyelination (Figures 2G and 2H). Axonal diameters between *Gde2KO* animals and WT littermates were comparable (Figure 2I), suggesting that the decrease in myelin thickness observed in *Gde2KO* animals is not a consequence of altered axon caliber. These collective observations suggest that GDE2 is required for promoting OL maturation during the peak period of developmental myelination in postnatal brain. By P28, numbers of $ASPA^+$ myelinating OLs and levels of MBP and MOG proteins in *Gde2KO* animals had normalized to WT

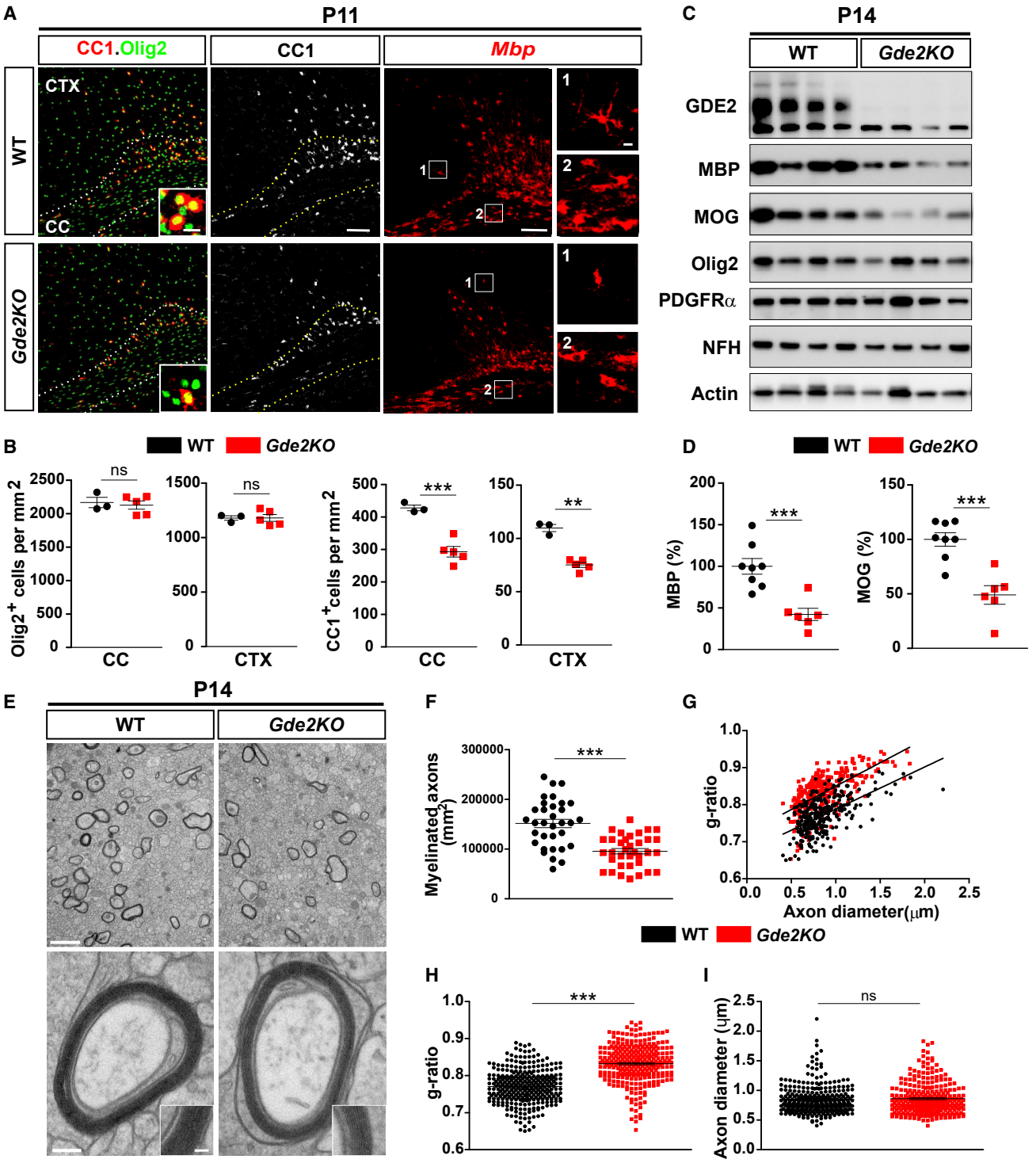

Figure 2. GDE2 Ablation Impairs OL Maturation

(A) Coronal sections of motor CTX and CC. Hatched lines mark the CC. Insets and boxed areas show high magnification in the corresponding panels.

(B) Graphs quantifying Olig2$^+$ and CC1$^+$ cells in CC and CTX. Nonsignificant (ns), $p > 0.05$; ***$p = 0.0007$; **$p = 0.0035$. n = 3 WT, n = 5 *Gde2KO*.

(C) Western blot of cortical extracts. Actin was used as a loading control (Olig2, $p = 0.1745$; PDGFRα, $p = 0.5163$).

(D) Graphs quantifying western blots for MBP (***$p = 0.0005$) and MOG (***$p = 0.0009$). n = 8 WT, n = 6 *Gde2KO*.

(E) TEM of CC.

(legend continued on next page)

amounts, suggesting that the loss of GDE2 results in delayed OL maturation (Figures S3C–S3E). However, EM analysis of 10-week animals showed that in contrast to WT, there was a dramatic reduction in myelinated larger-diameter axons in *Gde2KO* animals, although the incidence and myelination of smaller-diameter axons were normal (Figure S3F). This observation suggests that the temporal control of OL maturation by GDE2 is necessary for appropriate axonal myelination.

Neuronal GDE2 Promotes OL Maturation

GDE2 is predominantly expressed in neurons, suggesting that GDE2 acts non-cell autonomously to regulate the timing of OL maturation. To test this hypothesis, we used Cre-lox genetics to ablate GDE2 function in neurons. *Nex-Cre* mice express Cre recombinase under the control of the endogenous promoter of the NEX transcription factor, which targets Cre expression in cortical excitatory pyramidal neurons and hippocampus, but not in proliferating neural progenitors, interneurons, OLs, or astrocytes (Goebbels et al., 2006). Thus, *Gde2-$^{lox/-}$;Nex-Cre* mice (N-*Gde2KO*) will lack GDE2 expression and function in pyramidal neurons but retain GDE2 OL function. Western blot of P14 cortical extracts shows that GDE2 expression is reduced by ~80% in N-*Gde2KO* condition compared with *Gde2*$^{+/-}$; *Nex-Cre* controls (*Ctrl*) (Figures 3E and 3F). This confirms efficient ablation of GDE2 expression and supports our earlier observation that GDE2 expression is predominantly neuronal (Figure 1). N-*Gde2KO* showed no differences in the number of NG2/Olig2 cells, confirming that neuronal GDE2 does not influence OPC production (Figures 3A and 3B). However, N-*Gde2KO* animals showed a 15% reduction in Olig2$^+$ CC1$^+$ OLs in the CC and a more marked 30% reduction of Olig2$^+$ CC1$^+$ OLs in the CTX compared with controls (Figures 3C and 3D). In addition, western blot of P14 cortical extracts showed robust reduction of MBP and MOG in N-*Gde2KO* mice compared with control littermates (Figures 3E and 3F). Both genotypes showed equivalent levels of Olig2 and PDGFRα, which are expressed primarily in oligodendroglial cells and OPCs respectively, suggesting that overall numbers of oligodendroglia are not disrupted in N-*Gde2KO* animals (Figure 3E). Moreover, the amounts of axonal Neurofilament Heavy Chain (NFH) protein is similar between N-*Gde2KO* and control animals confirming earlier observations that cortical neuronal numbers and lamination are grossly intact in both cases (Figure 3E). Taken together, our observations in N-*Gde2KO* brain recapitulate the OL phenotypes of *Gde2KO* animals and provide genetic evidence that GDE2 neuronal function is required to promote OL maturation.

Neuronal GDE2 Releases Factors to Promote OL Maturation

To define the mechanisms by which neuronal GDE2 enhances OL maturation, we co-cultured purified WT and *Gde2KO* neurons with WT OPCs. Cortical neurons were derived from embryonic day 16.5 (E16.5) embryos and cultured for 3 days *in vitro* (DIV3); at this stage, neurons are immature and are undergoing active axonal and dendritic growth similar to neurons in postnatal brain at the time of OL maturation. WT and *Gde2KO* neuronal cultures were equivalent and typically composed of 95% neurons (β-tubulin type III$^+$) and ~2% astrocytes (GFAP$^+$), with no Olig2$^+$ oligodendroglia (Figure S4A). On DIV3, OPCs purified from P6 WT cortices were plated on WT and *Gde2KO* neurons in the absence of mitogenic factors and co-cultured for an additional 3 days (Figure 4A). Cultures were then fixed and examined for OL maturation. When compared with OPCs cocultured with WT neurons, OPCs cocultured with *Gde2KO* neurons showed a 33% reduction in the number of mature MBP$^+$ OLs (Figure 4B), and the number of myelinated segments in 9-day co-cultures was markedly reduced (Figure 4B). Total numbers of Olig2$^+$ OL lineage cells were equivalent between the two conditions (Figure S4B). These observations recapitulate our *in vivo* data indicating that GDE2 neuronal function is required for OL maturation.

We next treated freshly purified WT OPCs with conditioned medium (CM) collected from WT or *Gde2KO* neurons at DIV3 and DIV4 (Figure 4C). Specifically, WT OPCs were cultured for 1 day in DIV3 CM and on the next day cultured with CM collected between DIV3 and DIV4 for 2 days and then fixed and analyzed for OL maturation (Figure 4C). The total number of MBP$^+$ OLs in cultures treated with *Gde2KO* CM was reduced by ~25% compared with WT CM (Figure 4D; Table S1). CM prepared from DIV3 WT and *Gde2KO* neurons alone recapitulated these changes in OL maturation (Figure 4D; Table S1). These observations suggest that neuronal GDE2 does not utilize contact-mediated signals to regulate OL maturation. Instead, GDE2 stimulates the release of soluble OL maturation factors, and these factors are released by DIV3 neurons.

OLs *in vitro* undergo stereotypic morphological changes, increase expression of myelin proteins, and shift from actin assembly to disassembly coincident with myelination (Zuchero et al., 2015). We defined three stages of OL maturation based on their morphology, MBP expression, and F-actin network visualized by phalloidin staining (Figure 4E; Zuchero et al., 2015). Differentiating Olig2$^+$ OLs *in vitro* are arborized, with weak cell-body MBP expression and robust phalloidin labeling in the cell body and distal processes (stage 1, immature). Partially differentiated OLs show strong MBP expression and phalloidin labeling in distal processes, with occasional flattening of the myelin sheath in distal structures (stage 2, premyelinating), while more mature OLs show ring-like or lamellar morphology with increased MBP expression throughout the membrane sheath with near absence of the actin cytoskeleton (stage 3, myelinating). WT OPCs co-cultured with *Gde2KO* neurons after DIV3 showed a 40% and 50% reduction in the number of OLs at stages 2 and 3 of maturation and an ~25% reduction in the number of OLs at stage 1 (Figure 4F; Table S1). Similarly, WT OPCs

(F–I) Graphs quantifying myelinated axons (F) (***$p < 0.0001$, points represent individual regions of interest [ROIs]), g-ratios (G and H) (***$p < 0.0001$, points represent individual myelinated axons), and axon diameter (I) (ns, $p = 0.5523$). n = 3 WT, 3 *Gde2KO*.
All graphs show mean ± SEM, two-tailed unpaired Student's t test. Scale bars represent 100 μm (A) (insets, 5 μm), 2 μm (E, top), and 100 nm (E, bottom) (inset, 50 nm).

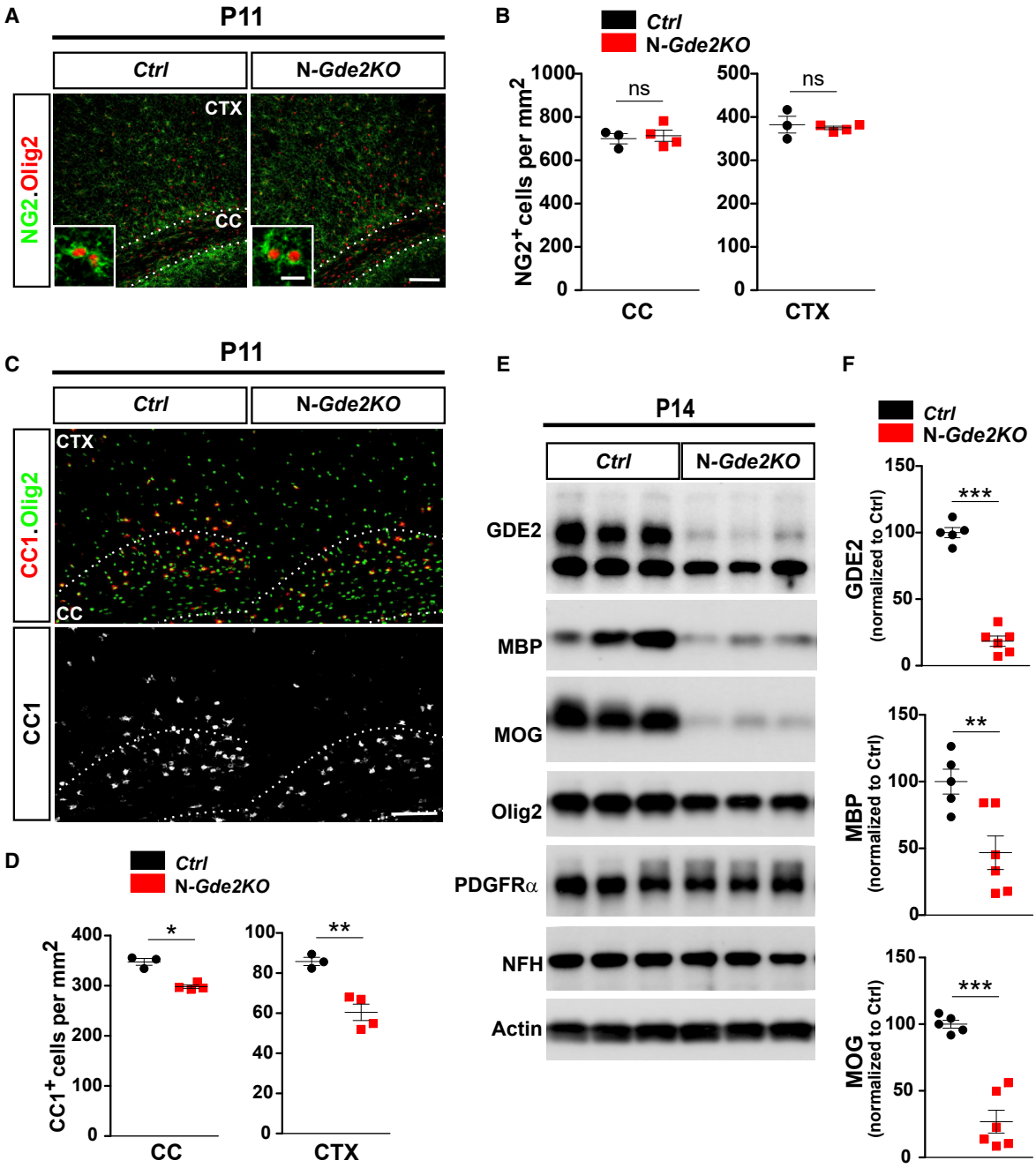

Figure 3. Neuronal GDE2 Promotes OL Maturation

(A and C) Coronal sections of motor CTX and CC showing NG2 (A) and CC1 (C) expression with Olig2 . Hatched lines mark the CC. *Ctrl*: *Gde2*$^{+/-}$*;Nex-Cre* N-*Gde2KO*: *Gde2*$^{lox/-}$*;Nex-Cre*.

(B and D) Graphs quantifying NG2^{+} OPCs and CC1^{+} cells in CC and CTX. (B) ns $p > 0.05$, (D) *$p = 0.0227$, **$p = 0.0052$. n = 3 *Ctrl*, 4 N-*Gde2KO*.

(E) Western blot of cortical extracts. Actin was used as a loading control. Levels of Olig2 ($p = 0.5804$) and PDGFRα ($p = 0.4708$) are unchanged between genotypes.

(F) Graphs quantifying western blots (GDE2, ***$p < 0.0001$; MBP, **$p = 0.0091$; MOG, ***$p = 0.0002$). n = 5 *Ctrl*, n = 6 N-*Gde2KO*.

All graphs show mean ± SEM, two-tailed unpaired Student's t test. Scale bars represent 100 μm (A and C), 10 μm (inset A).

grown in DIV3+4 CM showed a 25% and 50% reduction in the number of OLs at stages 2 and 3 of maturation when treated with *Gde2KO* CM but no change in the number of stage 1 OLs (Figure 4F; Table S1). These observations suggest that GDE2-dependent pathways in neurons release factors that promote OL maturation.

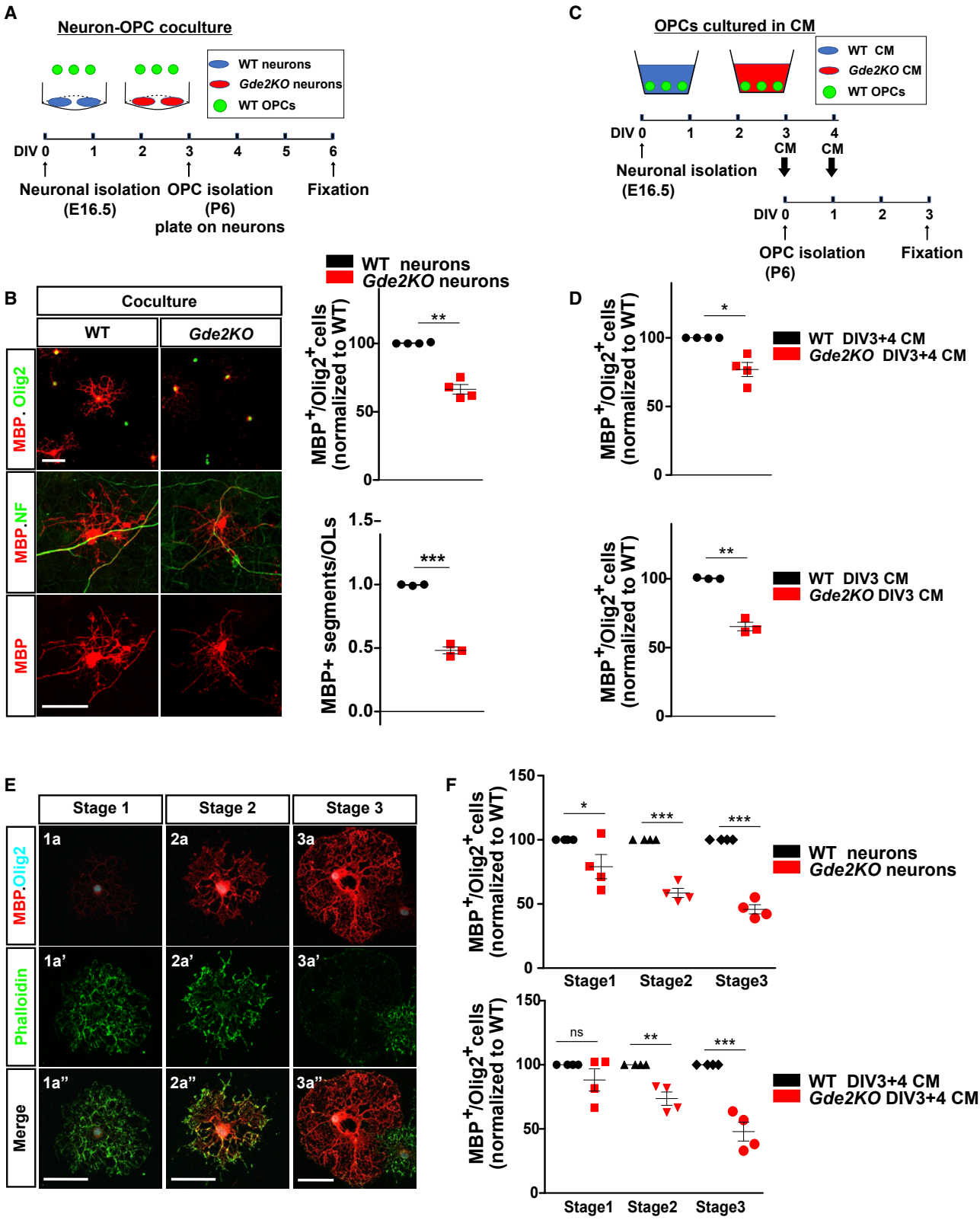

(legend on next page)

Neuronal activity is a central driver of OL maturation. We utilized optical recording of intracellular calcium via the calcium indicator Fluo-4 to monitor neuronal activity in cultured WT and *Gde2KO* neurons at DIV3 (Figure S4C), when cultured neurons utilize GDE2 pathways to release factors required for OL maturation. Analysis of calcium transients (ΔF/Fo) over a 3.5-min recording period showed no detectable calcium transients in DIV3 WT and *Gde2KO* neurons (Figure S4C). Treatment with the ionophore ionomycin, which ensures calcium internalization, results in robust signal confirming efficient Fluo-4 loading in neurons. These observations indicate that DIV3 WT and *Gde2KO* neurons are immature and largely inactive at this stage, suggesting that GDE2 regulation of OL maturation is unlikely to involve neuronal activity-dependent mechanisms. Stimulation of cultured neurons through addition of bicuculline did not alter GDE2 protein levels, supporting activity-independent roles for GDE2 in regulating OL maturation (Figure S4D).

GDE2 Maintains Canonical Wnt Signaling in Neurons

To gain insight into potential pathways that mediate GDE2 control of OL maturation, we performed bulk RNA sequencing (RNA-seq) of WT and *Gde2KO* nervous system tissue. 454 genes were differentially expressed in *Gde2KO* tissues compared with WT (Table S2), and Gene Ontology (GO) analysis using the STRING database (v.11) highlighted pathways associated with canonical Wnt signaling (Figures S5A and S5B). Known canonical Wnt target genes (https://web.stanford.edu/group/nusselab/cgi-bin/wnt/target_genes) were downregulated in the *Gde2KO* condition, implying that GDE2 normally potentiates Wnt pathway activation (Figure S5C). Wnt ligands bind their cognate receptors to ultimately stabilize and promote nuclear translocation of β-catenin (Janda et al., 2012). Nuclear, activated β-catenin (ABC) interacts with transcription factors to regulate expression of Wnt target genes, which include the transcription factor *Lef1* (Hovanes et al., 2001; Shimogori et al., 2004). qPCR analysis showed a 32% reduction in *Lef1* expression in cDNAs prepared from P10 *Gde2KO* cortical tissue compared with WT, and this decrease was recapitulated in *Gde2KO* cultured cortical neurons (Figure 5A). Further, levels of ABC detected by antibodies specific to β-catenin that is dephosphorylated on residues Ser37 or Thr41 (Liu et al., 2002) are decreased in *Gde2KO* DIV3 neuronal extracts compared to WT, while total levels of β-catenin are unchanged (Figure 5B). Immunohistochemical and biochemical analyses reveal that ABC levels in both nuclear and cytoplasmic compartments of *Gde2KO* DIV3 neurons are decreased (Figures 5C and 5D). These observations suggest that canonical Wnt signaling in neurons is reduced when neuronal GDE2 function is disrupted.

We next examined the temporal and spatial pattern of canonical Wnt pathway activation *in vivo* using a mouse reporter line that visualizes *in situ* Wnt pathway activation through expression of EGFP (*Rosa26 Tcf./Lef-H2B-EGFP* mice or *Wnt-EGFP*) (Cho et al., 2017). Analysis of *Wnt-EGFP* mice at P7 and P11 show robust nuclear EGFP expression in neurons and Olig2$^+$ cells, coincident with the period of OL maturation (Figures S5D and S5E). In contrast, little to no neuronal GFP expression is detected at P28 when developmental myelination is almost complete. However, GFP continues to be expressed in ~20% of Olig2$^+$ cells (Figures S5D and S5E). Thus, Wnt activation in WT neurons overlaps with GDE2 neuronal expression and the temporal profile of GDE2 requirement in OL maturation.

To determine if Wnt signaling is dependent on GDE2 expression, we introduced the *Wnt-EGFP* reporter into *Gde2KO* animals. Total numbers of GFP$^+$ cells were reduced in *Gde2-KO;Wnt-EGFP* animals compared with WT controls, suggesting reduced Wnt pathway activation in the absence of GDE2 (Figures S5F and S5G). *Gde2KO;Wnt-EGFP* animals showed a marked 40% reduction in the number of EGFP-expressing neurons (NeuN$^+$) compared with WT littermates (Figures 5E and 5F). This indicates that GDE2 is required to maintain canonical Wnt signaling in neurons at the time of OL maturation. P11 *Gde2KO;Wnt-EGFP* cortices also show 25% and 40% reduced EGFP expression in oligodendroglia (Olig2$^+$ cells) in CC and CTX, respectively (Figures 5G and 5H). The numbers of neurons and oligodendroglia were equivalent in both *Wnt-EGFP* and *Gde2KO;Wnt-EGFP* animals (Figures 5E–5H). NG2 progenitors show robust GFP expression while immature (TCF4$^+$ CC1$^-$) and mature (TCF4$^-$ CC1$^+$) OLs show minimal EGFP expression, suggesting that Wnt activity is restricted to OPCs (Figure S5H). Because GDE2 is expressed in OLs and not OPCs, this implies that GDE2-dependent activation of Wnt signaling in OPCs is non-cell autonomous. These observations indicate that GDE2 maintains canonical Wnt activity in neurons and OPCs at the time of OL maturation in the developing postnatal CTX.

Increasing Neuronal Wnt Activity in *Gde2KO* Mice Rescues OL Maturation

To test if the reduction in canonical Wnt activity is causal for OL maturation deficits in *Gde2KOs*, we increased Wnt signaling in *Gde2KO* animals by genetically stabilizing β-catenin *in vivo*. *Ctnnb1flex3* mice harbor *loxP* sites flanking exon 3 of β-catenin

Figure 4. GDE2 Releases Neuronally Derived Factors that Promote OL Maturation

(A) Schematic of neuron-OPC co-culture.

(B) WT OPCs co-cultured with WT or *Gde2KO* neurons. Graphs quantifying the percentage of MBP$^+$ Olig2$^+$ OLs (normalized to WT) (**p = 0.0019, n = 4 WT, n = 4 *Gde2KO*) and numbers of MBP$^+$ segments (***p < 0.0001, n = 3 WT, 3 *Gde2KO*).

(C) Schematic of OPCs cultured with neuronal conditioned medium (CM) (DIV3+4 CM).

(D) Graphs quantifying percentage of MBP$^+$ Olig2$^+$ OLs (normalized to WT). DIV3+4 CM, *p = 0.0209, n = 4 WT, n = 4 *Gde2KO* CM; DIV3 CM, **p = 0.0078, n = 3 WT, n = 3 *Gde2KO* CM.

(E) Representative images of the three stages of OL maturation *in vitro*.

(F) Graphs quantifying percentage of MBP$^+$ Olig2$^+$ OLs. Top: co-culture two-way ANOVA ***p < 0.0001 (Bonferroni correction), *p < 0.05, ***p < 0.001; n = 4 WT, n = 4 *Gde2KO*. Bottom: WT OPCs cultured with CM, two-way ANOVA ***p < 0.0001 (Bonferroni correction); ns, p > 0.05; **p < 0.01; ***p < 0.001; n = 4 WT, n = 4 *Gde2KO* CM.

All graphs show mean ± SEM (B and D), two-tailed unpaired Student's t test. Scale bars represent 50 μm (B and E). See Table S1 for cell numbers.

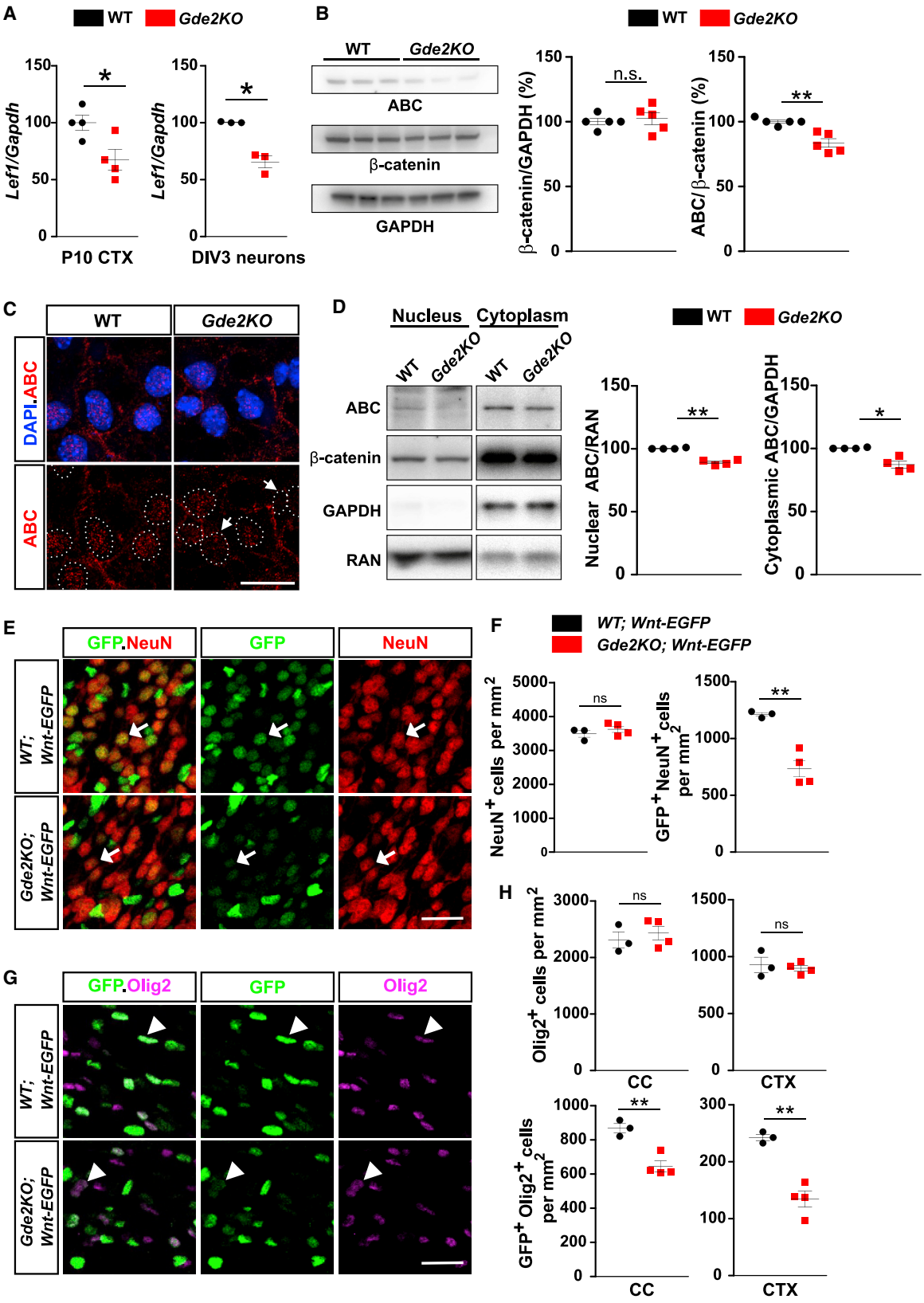

(legend on next page)

(*β-cat*^{ex3}), which contains phosphorylation sites for GSK3-β that target β-catenin for degradation (Harada et al., 1999). Cre-dependent excision of exon 3 prevents GSK3-β phosphorylation of β-catenin, thus stabilizing β-catenin and increasing canonical Wnt signaling. We first stabilized β-catenin in neurons of *Gde2KO* mice by generating *Gde2KO;Nex-Cre;β-cat*^{ex3} animals (*Gde2KO;*N-*β-cat*^{ex3}). Western blots from P14 cortical extracts confirmed Cre-dependent removal of exon 3 in β-catenin protein in *Gde2KO;*N-*β-cat*^{ex3} animals, but not in *WT;β-cat*^{ex3} and *Gde2-KO;β-cat*^{ex3} controls (Figure S6A). All three genotypes had equivalent numbers of Olig2$^+$ cells, suggesting that β-catenin stabilization in neurons had minimal effect on the number of OL lineage cells (Figure S6B). However, there was a substantial increase of Olig2$^+$ *Mbp*$^+$ mature OLs in *Gde2KO;*N-*β-cat*^{ex3} cortices compared to *Gde2KO;β-cat*^{ex3} controls that restored numbers of mature Olig2$^+$ *Mbp*$^+$ OLs to WT levels (Figures 6A and 6B). *Gde2KO;*N-*β-cat*^{ex3} cortices also showed recovery of CC1$^+$ Olig2$^+$ OLs to WT levels in CC with partial rescue in CTX (Figures 6C and 6D). These observations suggest that GDE2 mediates OL maturation through stimulation of canonical Wnt signaling in neurons.

Gde2KO animals also display reduced Wnt signaling in OPCs (Figures 5G and 5H). We stabilized β-catenin in OPCs by generating *Gde2KO;β-cat*^{ex3}*;PDGFαR-CreER* animals (*Gde2KO;*O-*β-cat*^{ex3}), which express Cre recombinase in OPCs in response to 4 hydroxytamoxifen (4-HT) (Kang et al., 2010). We administered 4-HT to *Gde2KO;*O-*β-cat*^{ex3} mice and *WT;β-cat*^{ex3}and *Gde2KO;β-cat*^{ex3} controls at P7 and examined OL maturation at P11. β-Catenin stabilization in OPCs in *Gde2KO;*O-*β-cat*^{ex3} mice resulted in reduced numbers of Olig2$^+$ oligodendroglia in CC compared with controls, whereas Olig2$^+$ cells in CTX were equivalent between genotypes (Figures S7A and S7B). OL maturation was further retarded in both CC and CTX in *Gde2KO;*O-*β-cat*^{ex3} CTX (Figures S7C–S7E). Because OL maturation phenotypes are not rescued in *Gde2KO;*O-*β-cat*^{ex3} animals, we conclude that GDE2 regulation of canonical Wnt signaling in OPCs does not promote OL maturation.

Neuronal Wnt Activity Releases OL Maturation Factors

To test if GDE2 stimulation of Wnt signaling in neurons is required for the release of OL maturation factors, we generated CM from neurons isolated from *Gde2KO;β-cat*^{ex3} and *Gde2KO;*N-*β-cat*^{ex3} animals that were cultured till DIV3 (Figure 7A). WT OPCs were treated for 3 days with CM and examined for OL maturation. Strikingly, CM from *Gde2KO* neurons with stabilized β-catenin (*Gde2KO;*N-*β-cat*^{ex3}) showed an ~60% increase in the number of MBP$^+$ OLs compared with CM from *Gde2KO* neurons (*Gde2KO;β-cat*^{ex3}), as well as a robust increase in MBP protein by western blot (Figures 7A and 7B; Table S1). Further, we observed a 60% increase in the number of stage 1, stage2, and stage3 MBP$^+$ OLs in CM from *Gde2KO;*N-*β-cat*^{ex3} neurons compared with CM from *Gde2-KO;β-cat*^{ex3} condition (Figure 7B; Table S1). Thus, stabilization of β-catenin in *Gde2KO* neurons is sufficient to release factors that stimulate OL maturation. This is consistent with the model that GDE2 stimulates canonical Wnt signaling in neurons and that this pathway potentiates the release of neuronally derived factors that promote OL maturation. The increase in stage 1 OLs in the presence of CM from *Gde2KO* neurons with stabilized β-catenin contrasts with our observation that the production of stage 1 OLs is not dependent on GDE2 neuronal CM (Figures 7B and 4F). We attribute this to the robust and continuous release of OL maturation factors when β-catenin is constitutively stabilized in neurons.

Candidate Factors Released by GDE2/Wnt Signaling in Neurons

To identify OL maturation factors released by GDE2 neuronal function, we collected WT and *Gde2KO* CM and analyzed the protein content by mass spectrometry. We identified 149 proteins that were expressed at 40% or higher in *Gde2KO* CM compared to WT CM (Table S3). GDE2 releases GPI-anchored proteins from the plasma membrane; however, no GPI-anchored proteins were differentially expressed in WT and *Gde2KO* CM (Figure S8A). This is consistent with our model that GDE2 stimulates Wnt signaling in neurons, which drives the release of neuronal factors that promote OL maturation. We identified 11 secreted/extracellular matrix (ECM) associated proteins that were differentially expressed in WT and *Gde2KO* neuronal CM, with 10 proteins showing decreased expression in *Gde2KO* CM (Figure S8B). Of these 10 proteins, soluble receptor-type tyrosine-protein phosphatase zeta (RPTPzeta, or phosphacan) can promote OL maturation through interaction with contactin-1 in OPCs (Lamprianou et al., 2011). Phosphacan is expressed in neurons, astrocytes, and oligodendroglia (Cahoy et al., 2008; Dwyer et al., 2015); accordingly, released phosphacan is a promising candidate for mediating GDE2-dependent regulation of OL maturation. Neuronally derived phosphacan is distinguished from glial phosphacan by antibodies that recognize

Figure 5. Canonical Wnt Signaling Is Reduced in *Gde2KO* Neurons and Oligodendroglia

(A) Graphs quantifying qPCR of *Lef1* transcripts normalized to *Gapdh* mRNAs. CTX, *p = 0.0231, n = 4 WT, n = 4 *Gde2KO*; DIV3 cortical neurons, *p = 0.0362, n = 3 WT, n = 3 *Gde2KO*.

(B) Western blot of DIV3 cortical neurons with associated quantification. ns, p = 0.6465; **p = 0.0018; n = 5 WT, n = 5 *Gde2KO*.

(C) Images of cultured cortical neurons. Arrows mark reduced ABC nuclear (hatched lines) staining.

(D) Western blot of fractionated DIV3 cortical neuron extracts. Graphs quantifying ABC normalized to RAN and GAPDH, **p = 0.0019, *p = 0.0186, n = 4 WT, n = 4 *Gde2KO*.

(E and G) Coronal sections of P11 CTX. (E) Arrows show differential GFP expression in neurons in WT and *Gde2KO;Wnt-EGFP* mice. (G) Arrowheads mark differential GFP expression in Olig2$^+$ cells in WT and *Gde2KO;Wnt-EGFP* mice.

(F) Graphs quantifying neurons and GFP$^+$ neurons in WT and *Gde2KO;Wnt-EGFP* mice. ns, p = 0.3936; **p = 0.0078.

(H) Graphs quantifying Olig2$^+$ and GFP$^+$ Olig2$^+$ cells in WT and *Gde2KO;Wnt-EGFP* mice. ns, p > 0.05, CC **p = 0.006, CTX **p = 0.0057. For (F) and (H), n = 3 *WT;Wnt-EGFP*, 4 *Gde2KO;Wnt-EGFP*.

All graphs show mean ± SEM, two-tailed unpaired Student's t test. Scale bars represent 5 μm (C) and 20 μm (E and G).

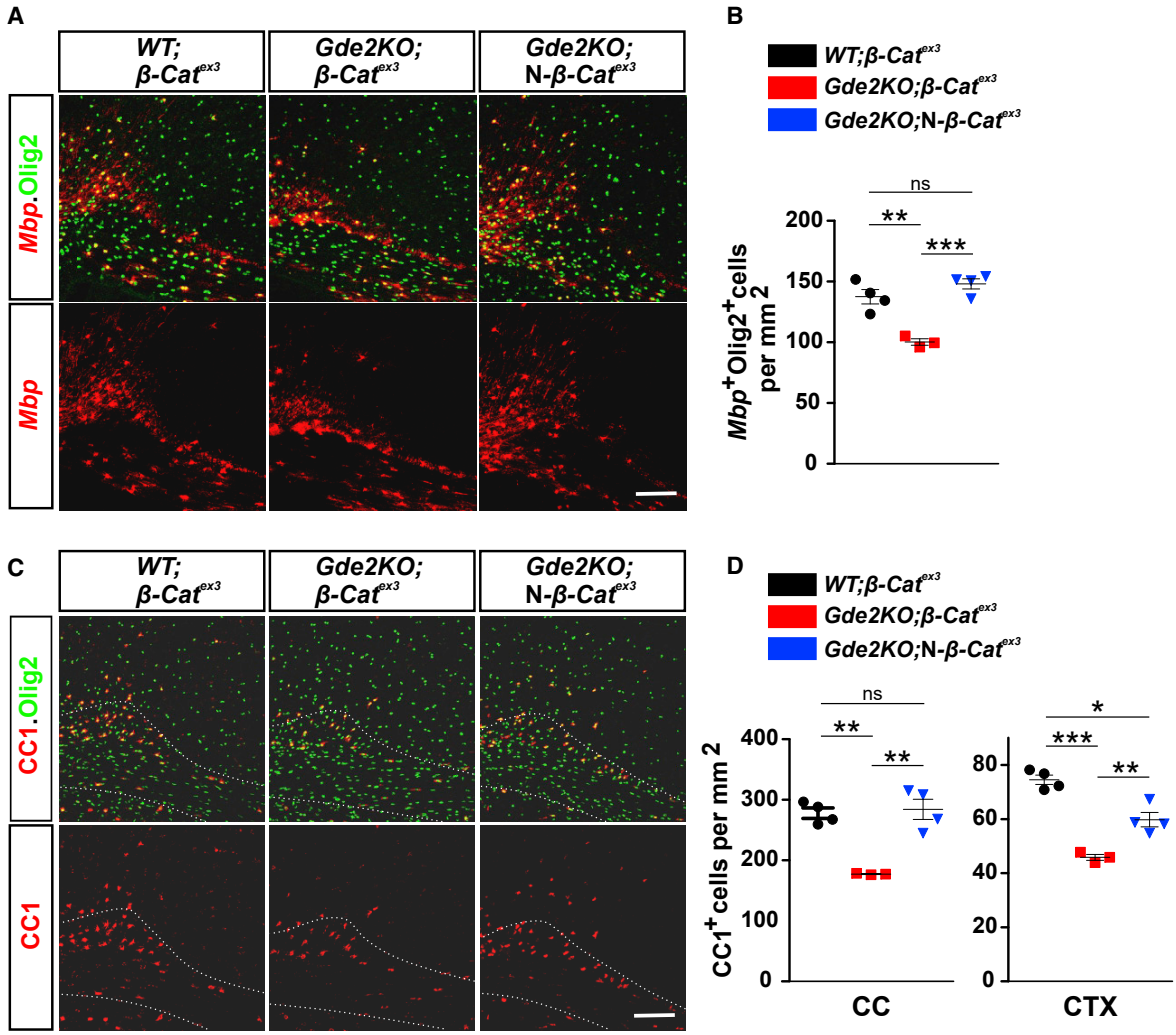

Figure 6. Stabilizing β-Catenin in Neurons Rescues *Gde2KO* OL Maturation

(A and C) Coronal sections of motor CTX and CC showing expression of Mbp (A) and CC1 (C) expression in oligodendroglia (Olig2$^+$). Hatched lines mark the CC.

(B) Graph quantifying Olig2$^+$ cells expressing *Mbp* transcripts. **p = 0.0047, ***p = 0.0006, ns = 0.204.

(D) Graph quantifying numbers of CC1$^+$ OLs. In CC, **p = 0.0014 (*WT;β-cat^{ex3}* versus *Gde2KO;β-cat^{ex3}*), **p = 0.0078 (*Gde2KO;β-cat^{ex3}* versus *Gde2KO;*N-*β-cat^{ex3}*), ns p = 0.7592 (*WT;β-cat^{ex3}* versus *Gde2KO;*N-*β-cat^{ex3}*). In CTX, ***p = 0.0006 (*WT;β-cat^{ex3}* versus *Gde2KO;β-cat^{ex3}*), **p = 0.0098 (*Gde2KO;β-cat^{ex3}* versus *Gde2KO;*N-*β-cat^{ex3}*), *p = 0.0156 (*WT;β-cat^{ex3}* versus *Gde2KO;*N-*β-cat^{ex3}*). n = 4 *WT;β-cat^{ex3}*, 3 *Gde2KO;β-cat^{ex3}*, n = 4 *Gde2KO;*N-*β-cat^{ex3}*.

All graphs show mean ± SEM, two-tailed unpaired Student's t test. Scale bars represent 100 μm (A and C).

cell-type-specific O-mannosyl glycans (Dwyer et al., 2015). Western blots reveal that levels of neuronal phosphacan are reduced in *Gde2KO* CM compared to WT. In contrast, GPI-anchored protein TAG1 levels are equivalent between conditions (Figure 7C). These observations confirm the proteomic analysis of phosphacan and Tag1 expression in *Gde2KO* and WT CM (Figures S8A and S8B). To determine if reduced levels of phosphacan mediate the delay in OL maturation exerted by *Gde2KO* CM, we depleted phosphacan from WT CM using antibodies to neuronal phosphacan conjugated to protein L (Figure S8C). OPCs cultured with phosphacan depleted CM largely recapitulated the delay in OL maturation elicited by *Gde2KO* CM; specifically, the number of MBP$^+$ cells was decreased with concomitant reductions in stage 1, stage 2, and stage 3 MBP$^+$ OLs (Figures S8D and S8E; Table S1). The degree of OL maturation was not changed when WT CM incubated with protein L alone was used (Figure S8E; Table S1). Our genetic studies suggest that GDE2 stimulation of canonical Wnt signaling in neurons mediates OL maturation. We thus performed western blot analysis on CM prepared from *Gde2KO;*N-*β-cat^{ex3}* and *Gde2-KO;β-cat^{ex3}* neuronal cultures. Levels of soluble neuronally derived phosphacan were markedly increased in CM from *Gde2KO;*N-*β-cat^{ex3}* cortical cultures compared with control *Gde2KO;β-cat^{ex3}* CM (Figure 7D). These observations suggest that GDE2 stimulation of Wnt signaling in neurons releases soluble factors, such as phosphacan, that promote OL maturation.

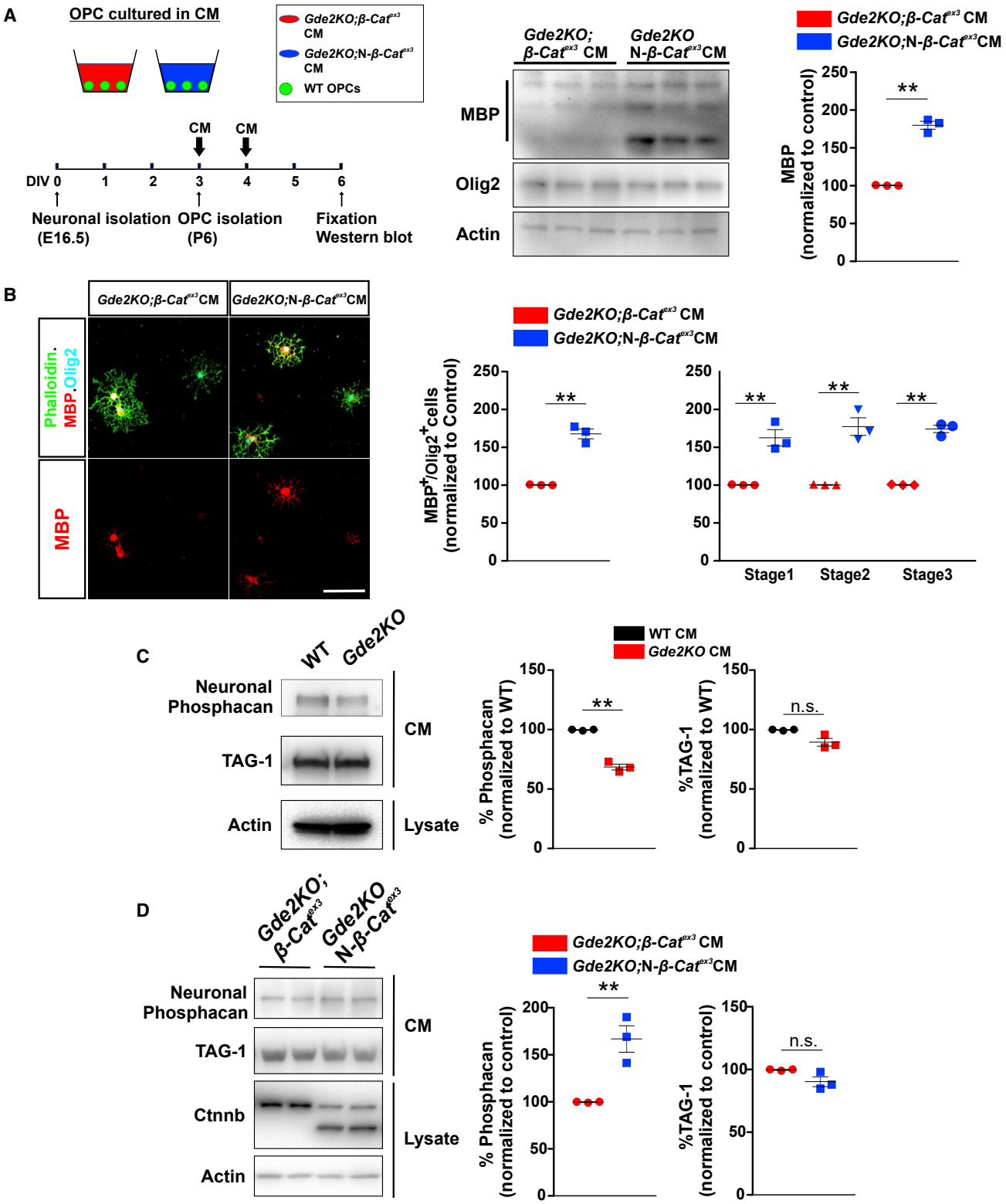

Figure 7. Stabilized β-Catenin in Neurons Stimulates Release of OL Maturation Factors

(A) Schematic of OPCs cultured with neuronal CM. Western blot of WT OPC lysates + CM and MBP quantification. **p = 0.0043, n = 3 *Gde2KO;β-cat*^{ex3}, n = 3 *Gde2KO;*N-*β-cat*^{ex3}CM.

(legend continued on next page)

DISCUSSION

Our studies reveal that GDE2 neuronal function promotes the maturation of premyelinating OLs in the developing CTX. During the period of developmental myelination, GDE2 is predominantly expressed in cortical neurons, where it is required to maintain canonical Wnt signaling. Activation of canonical Wnt pathways causes the release of soluble factors from neurons such as phosphacan that promote the production of premyelinating and myelinating OLs from OPCs (Figure S8F). These observations identify roles for neuronal GDE2 in regulating OL maturation and suggest that GDE2 regulation of Wnt signaling in neurons is part of the complex interplay between neurons and glia that coordinates axonal myelination during cortical development.

Neuronal GDE2 and OL Maturation

Known factors in neurons that regulate OL development include contact-dependent signals between axons and oligodendroglia, axon caliber, and neuronal activity (Charles et al., 2000; Gibson et al., 2014; Lee et al., 2012). Here, we show that GDE2 activity in neurons stimulates OL maturation through pathways that are apparently separate from these mechanisms. Our studies using WT and *Gde2KO* neuronal CM suggest that GDE2 regulates OL maturation through the release of soluble promaturation factors and not through contact-mediated pathways. Further, CM with promaturation activity was derived from DIV3 cultured neurons that are immature and lack obvious neuronal activity, as assayed by calcium imaging, thus ruling out possible contributions of activity-dependent mechanisms. In addition, measurements of axonal diameters indicate that axonal caliber is unaffected by disruption of GDE2 function. Our studies provide support for a mechanism driven by GDE2, whereby neurons release soluble factors that promote nearby OPCs to differentiate and initiate the myelination program. This idea is consistent with the expression of GDE2 in the developing CTX, which matches the pattern of OL maturation and myelination that initiates in deep layers and broadens to the superficial laminae (Tomassy et al., 2014). We note that GDE2 loss leads to a delay in OL maturation; by P28, the numbers of myelinating OLs and myelin-associated proteins in *Gde2KO* animals are equivalent to WT. This recovery is likely due to the robust compensatory mechanisms known to occur when OL development is disrupted. However, the increased incidence of unmyelinated large-diameter axons in *Gde2KO* adult animals suggests that the timing of OL maturation regulated by GDE2-dependent mechanisms is important to ensure appropriate axonal myelination. GDE2 is vertebrate specific (Nogusa et al., 2004). We speculate that GDE2 could constitute one of several regulatory pathways that have evolved in vertebrates to myelinate axons in order to facilitate complex neural circuit function.

GDE2 Regulation of Canonical Wnt Signaling and OL Maturation

Canonical Wnt signaling has established roles in cortical progenitor proliferation, differentiation, and neuronal migration (Bocchi et al., 2017; Chenn and Walsh, 2002; Munji et al., 2011). Our analysis of *Wnt-EGFP* reporter mice confirms Wnt signaling is active in neurons, OPCs, and OLs during the period of developmental myelination. By P28, when developmental myelination is almost complete, there is remarkably little Wnt activation in neurons, although subpopulations of oligodendroglial cells exhibit substantial reporter gene expression. We show here that Wnt activation in neurons and OPCs is dependent in part on GDE2 function. Activation of canonical Wnt signaling in OPCs in *Gde2KO* animals worsens OL maturation phenotypes and is consistent with previous studies showing that elevating Wnt signaling delays OL maturation and negatively regulates terminal OL differentiation (Fancy et al., 2009; Ye et al., 2009). In contrast, genetic stabilization of β-catenin in neurons of *Gde2KO* animals rescues their OL maturation phenotypes, indicating that GDE2-dependent maintenance of Wnt signaling in neurons is important for appropriate OL development. This observation identifies roles for neuronal canonical Wnt signaling in the cross-talk between neurons and oligodendroglia that coordinates the timing of OL maturation. While Wnt activation in neurons declines from P28, GDE2 continues to be expressed in neurons. This observation raises two main questions: how does GDE2 promote Wnt activation during developmental myelination, and how is this pathway switched off after P28? Greater insight into these questions will be gleaned from further investigation into the mechanisms by which GDE2 regulates canonical Wnt signaling. GDE2 is a membrane-bound enzyme that functions at the cell surface to regulate GPI-anchored protein function by cleavage of the GPI-anchor and release of the protein from the cell surface (Matas-Rico et al., 2016; Park et al., 2013). Accordingly, a plausible mechanism for GDE2 regulation of Wnt signaling is through regulation of GPI-anchored protein function. RECK and the heparan sulfate proteoglycans GPC6 and GPC4 are established substrates of GDE2 (Matas-Rico et al., 2016; Park et al., 2013). RECK can bind Wnt and can interact in a multiprotein complex with Gpr124 and Frizzled to stimulate Wnt signaling (Cho et al., 2017; Eubelen et al., 2018). GPC6 and GPC4 are known to regulate Wnt pathway activation and can function as activators or inhibitors of Wnt signaling (Han et al., 2005; Lebensohn et al., 2016; Sakane et al., 2012). The known contributions of RECK, GPC6, and GPC4 in the regulation of Wnt signaling warrant further investigation into whether they mediate GDE2-dependent control of OL maturation.

Neuronal Wnt Signaling Releases OL Maturation Factors from Neurons

Our studies suggest that GDE2 function in neurons is required for the release of soluble factors that promote OL maturation.

(B) Representative images of OPCs cultured in CM. Graphs quantifying the percentage of MBP^+ $Olig2^+$ cells. **p = 0.009. This increase spans all three stages of OL maturation: two-way ANOVA. ***p < 0.0001 (Bonferroni correction), **p < 0.001, n = 3 *Gde2KO;β-cat^{ex3}*, n = 3 *Gde2KO;*N-*β-cat^{ex3}* CM. See Table S1 for cell numbers.

(C) Western blot and protein quantification. **p = 0.0062; ns, p = 0.0864. n = 3 WT, n = 3 *Gde2KO* CM.

(D) Western blot and protein quantification. **p = 0.009; ns, p = 0.0781. n = 3 *Gde2KO;β-cat^{ex3}*, n = 3 *Gde2KO;*N-*β-cat^{ex3}*CM.

All graphs show mean ± SEM, two-tailed unpaired Student's t test. Scale bar represents 20 μm (B).

Strengthening the idea that GDE2 activation of canonical Wnt signaling mediates this release is that CM from *Gde2KO* neurons expressing stabilized β-catenin promotes OL maturation to an extent that is more potent than WT neuronal CM. Our proteomic analysis of WT and *Gde2KO* CM identified phosphacan within a cohort of secreted and ECM-associated proteins that were reduced in *Gde2KO* CM. Phosphacan is a splice variant of PTPRzeta encoded by the *Ptprz1* gene. It contains the extracellular domain of the full-length membrane-bound isoform of PTPRzeta that consists of an N-terminal carbonic anhydrase like domain, three fibronectin type III repeats, and attachment sites for chondroitin sulfate proteoglycan (Maurel et al., 1994). Loss of PTPRzeta results in increased OPC proliferation and impaired OL differentiation, and studies of cultured OPCs indicate that phosphacan regulates the rate of OL maturation via interaction with contactin-1 (Harroch et al., 2002; Lamprianou et al., 2011). PTPRzeta is widely expressed during developmental myelination, but the relevant cellular source for phosphacan that regulates OL maturation has not been defined (Faissner et al., 2006). We find that *Gde2KO* CM has reduced levels of neuronal phosphacan and that phosphacan levels are restored in CM prepared from *Gde2KO* neurons with stabilized β-catenin. Further, WT neuronal CM depleted for phosphacan mimics OL maturation deficits observed when OPCs are incubated with *Gde2KO* CM. These observations support the model that phosphacan released by GDE2-dependent activation of Wnt signaling in neurons mediates OL maturation. How Wnt signaling promotes phosphacan release is not clear. Phosphacan transcripts are not altered in our bulk RNA-seq data from *Gde2KO* tissue, favoring models that involve secondary mechanisms that impact phosphacan protein production and secretion. We have focused here on phosphacan because it is exemplar of a factor with known activities in promoting OL maturation. Given that CM is a complex mixture of proteins and RNA species, it is possible that Wnt signaling pathways in neurons promotes the release of additional factors important for OL maturation.

In summary, we have identified GDE2 regulation of canonical Wnt signaling in neurons as a pathway that controls the rate of OL maturation through the release of soluble promaturation factors that include phosphacan. This study provides insight into the complex communication pathways between axons and oligodendroglia that collectively regulate developmental myelination.

STAR★METHODS

Detailed methods are provided in the online version of this paper and include the following:

- KEY RESOURCES TABLE
- RESOURCE AVAILABILITY
  - Lead Contact
  - Materials Availability
  - Data and Code Availability
- EXPERIMENTAL MODEL AND SUBJECT DETAILS
  - Mice
- METHOD DETAILS
  - Tissue processing and immunohistochemistry
  - 4-HT preparation and administration
  - Fluorescent *in situ* hybridization (FISH)
  - Transmission Electron Microscopy (TEM)
  - Cell culture
  - Immunocytochemistry
  - Calcium transient imaging and analysis
  - mRNA-sequencing analysis
  - Mass spectrometry analysis
  - Immunoblotting
  - Quantitative real-time PCR
- QUANTIFICATION AND STATISTICAL ANALYSIS

SUPPLEMENTAL INFORMATION

Supplemental Information can be found online at https://doi.org/10.1016/j.celrep.2020.107540.

ACKNOWLEDGMENTS

We thank C. Wladyka and Y. Li for technical assistance; Drs. D. Bergles, P. Calabresi, and S. Bouyain and the Sockanathan lab for discussions; L. Florea for bioinformatics; Drs. J. Nathans (*Rosa26 Tcf/Lef H2B-EGFP*), M. Taketo (*Ctnnb1flex3/+*), K. Nave (*Nex:Cre*), and D. Bergles (*PDGFαR-CreER*) for mice; and the Multiphoton Imaging Core of the Johns Hopkins P30 Center for Neuroscience Research (NS050274). B.-R.C. was supported by a Fulbright Graduate Study Award (Science and Engineering). This work was supported by the National Institutes of Health (grant R01NS046336 to S.S.).

AUTHOR CONTRIBUTIONS

B.C. and S.S. conceived the project. B.C. performed all experiments except for RNA-seq (C.C.) and mass spectrometry studies (C.H.N.). B.C. and S.S. designed the experiments, interpreted the results, compiled and archived data, and wrote the manuscript. All authors read, edited, and contributed to the final version of the manuscript.

DECLARATION OF INTERESTS

The authors declare no competing interests.

Received: August 16, 2019
Revised: March 9, 2020
Accepted: March 28, 2020
Published: May 5, 2020

REFERENCES

Andrews, S. (2010). FastQC: a quality control tool for high throughput sequence data, Available at. http://www.bioinformatics.babraham.ac.uk/projects/fastqc.

Badea, T.C., Wang, Y., and Nathans, J. (2003). A noninvasive genetic/pharmacologic strategy for visualizing cell morphology and clonal relationships in the mouse. J. Neurosci. *23*, 2314–2322.

Barres, B.A., and Raff, M.C. (1993). Proliferation of oligodendrocyte precursor cells depends on electrical activity in axons. Nature *361*, 258–260.

Barres, B.A., Schmid, R., Sendnter, M., and Raff, M.C. (1993). Multiple extracellular signals are required for long-term oligodendrocyte survival. Development *118*, 283–295.

Baxi, E.G., DeBruin, J., Tosi, D.M., Grishkan, I.V., Smith, M.D., Kirby, L.A., Strasburger, H.J., Fairchild, A.N., Calabresi, P.A., and Gocke, A.R. (2015). Transfer of myelin-reactive th17 cells impairs endogenous remyelination in the central nervous system of cuprizone-fed mice. J. Neurosci. *35*, 8626–8639.

Bhat, R.V., Axt, K.J., Fosnaugh, J.S., Smith, K.J., Johnson, K.A., Hill, D.E., Kinzler, K.W., and Baraban, J.M. (1996). Expression of the APC tumor suppressor protein in oligodendroglia. Glia *17*, 169–174.

Bocchi, R., Egervari, K., Carol-Perdiguer, L., Viale, B., Quairiaux, C., De Roo, M., Boitard, M., Oskouie, S., Salmon, P., and Kiss, J.Z. (2017). Perturbed Wnt signaling leads to neuronal migration delay, altered interhemispheric connections and impaired social behavior. Nat. Commun. *8*, 1158.

Cahoy, J.D., Emery, B., Kaushal, A., Foo, L.C., Zamanian, J.L., Christopherson, K.S., Xing, Y., Lubischer, J.L., Krieg, P.A., Krupenko, S.A., et al. (2008). A transcriptome database for astrocytes, neurons, and oligodendrocytes: a new resource for understanding brain development and function. J. Neurosci. *28*, 264–278.

Cave, C., Park, S., Rodriguez, M., Nakamura, M., Hoke, A., Pletnikov, M., and Sockanathan, S. (2017). GDE2 is essential for neuronal survival in the postnatal mammalian spinal cord. Mol. Neurodegener. *12*, 8.

Charles, P., Hernandez, M.P., Stankoff, B., Aigrot, M.S., Colin, C., Rougon, G., Zalc, B., and Lubetzki, C. (2000). Negative regulation of central nervous system myelination by polysialylated-neural cell adhesion molecule. Proc. Natl. Acad. Sci. USA *97*, 7585–7590.

Chenn, A., and Walsh, C.A. (2002). Regulation of cerebral cortical size by control of cell cycle exit in neural precursors. Science *297*, 365–369.

Cho, C., Smallwood, P.M., and Nathans, J. (2017). Reck and Gpr124 are essential receptor cofactors for Wnt7a/Wnt7b-specific signaling in mammalian CNS angiogenesis and blood-brain barrier regulation. Neuron *95*, 1056–1073.e5.

Cox, J., and Mann, M. (2008). MaxQuant enables high peptide identification rates, individualized p.p.b.-range mass accuracies and proteome-wide protein quantification. Nat. Biotechnol. *26*, 1367–1372.

Davison, A.N., and Peters, A. (1970). Myelination (Charles C. Thomas), p. 56.

Dugas, J.C., Tai, Y.C., Speed, T.P., Ngai, J., and Barres, B.A. (2006). Functional genomic analysis of oligodendrocyte differentiation. J. Neurosci. *26*, 10967–10983.

Dwyer, C.A., Katoh, T., Tiemeyer, M., and Matthews, R.T. (2015). Neurons and glia modify receptor protein-tyrosine phosphatase ζ (RPTPζ)/phosphacan with cell-specific O-mannosyl glycans in the developing brain. J. Biol. Chem. *290*, 10256–10273.

Elbaz, B., Traka, M., Kunjamma, R.B., Dukala, D., Brosius Lutz, A., Anton, E.S., Barres, B.A., Soliven, B., and Popko, B. (2016). Adenomatous polyposis coli regulates radial axonal sorting and myelination in the PNS. Development *143*, 2356–2366.

Eubelen, M., Bostaille, N., Cabochette, P., Gauquier, A., Tebabi, P., Dumitru, A.C., Koehler, M., Gut, P., Alsteens, D., Stainier, D.Y.R., et al. (2018). A molecular mechanism for Wnt ligand-specific signaling. Science *361*, eaat1178.

Faissner, A., Heck, N., Dobbertin, A., and Garwood, J. (2006). DSD-1-proteoglycan/phosphacan and receptor protein tyrosine phosphatase-beta isoforms during development and regeneration of neural tissues. Adv. Exp. Med. Biol. *557*, 25–53.

Fancy, S.P., Baranzini, S.E., Zhao, C., Yuk, D.I., Irvine, K.A., Kaing, S., Sanai, N., Franklin, R.J., and Rowitch, D.H. (2009). Dysregulation of the Wnt pathway inhibits timely myelination and remyelination in the mammalian CNS. Genes Dev. *23*, 1571–1585.

Gibson, E.M., Purger, D., Mount, C.W., Goldstein, A.K., Lin, G.L., Wood, L.S., Inema, I., Miller, S.E., Bieri, G., Zuchero, J.B., et al. (2014). Neuronal activity promotes oligodendrogenesis and adaptive myelination in the mammalian brain. Science *344*, 1252304.

Goebbels, S., Bormuth, I., Bode, U., Hermanson, O., Schwab, M.H., and Nave, K.A. (2006). Genetic targeting of principal neurons in neocortex and hippocampus of NEX-Cre mice. Genesis *44*, 611–621.

Goebbels, S., Wieser, G.L., Pieper, A., Spitzer, S., Weege, B., Yan, K., Edgar, J.M., Yagensky, O., Wichert, S.P., Agarwal, A., et al. (2016). A neuronal PI(3,4,5)P3-dependent program of oligodendrocyte precursor recruitment and myelination. Nat Neurosci. *20*, 10–15.

Han, C., Yan, D., Belenkaya, T.Y., and Lin, X. (2005). Drosophila glypicans Dally and Dally-like shape the extracellular Wingless morphogen gradient in the wing disc. Development *132*, 667–679.

Harada, N., Tamai, Y., Ishikawa, T., Sauer, B., Takaku, K., Oshima, M., and Taketo, M.M. (1999). Intestinal polyposis in mice with a dominant stable mutation of the beta-catenin gene. EMBO J. *18*, 5931–5942.

Harroch, S., Furtado, G.C., Brueck, W., Rosenbluth, J., Lafaille, J., Chao, M., Buxbaum, J.D., and Schlessinger, J. (2002). A critical role for the protein tyrosine phosphatase receptor type Z in functional recovery from demyelinating lesions. Nat. Genet. *32*, 411–414.

Hovanes, K., Li, T.W., Munguia, J.E., Truong, T., Milovanovic, T., Lawrence Marsh, J., Holcombe, R.F., and Waterman, M.L. (2001). Beta-catenin-sensitive isoforms of lymphoid enhancer factor-1 are selectively expressed in colon cancer. Nat. Genet. *28*, 53–57.

Ishibashi, T., Dakin, K.A., Stevens, B., Lee, P.R., Kozlov, S.V., Stewart, C.L., and Fields, R.D. (2006). Astrocytes promote myelination in response to electrical impulses. Neuron *49*, 823–832.

Janda, C.Y., Waghray, D., Levin, A.M., Thomas, C., and Garcia, K.C. (2012). Structural basis of Wnt recognition by Frizzled. Science *337*, 59–64.

Kang, S.H., Fukaya, M., Yang, J.K., Rothstein, J.D., and Bergles, D.E. (2010). NG2+ CNS glial progenitors remain committed to the oligodendrocyte lineage in postnatal life and following neurodegeneration. Neuron *68*, 668–681.

Kessaris, N., Fogarty, M., Iannarelli, P., Grist, M., Wegner, M., and Richardson, W.D. (2006). Competing waves of oligodendrocytes in the forebrain and postnatal elimination of an embryonic lineage. Nat. Neurosci. *9*, 173–179.

Kim, S.Y., Adhikari, A., Lee, S.Y., Marshel, J.H., Kim, C.K., Mallory, C.S., Lo, M., Pak, S., Mattis, J., Lim, B.K., et al. (2013). Diverging neural pathways assemble a behavioural state from separable features in anxiety. Nature *496*, 219–223.

Kuhlbrodt, K., Herbarth, B., Sock, E., Hermans-Borgmeyer, I., and Wegner, M. (1998). Sox10, a novel transcriptional modulator in glial cells. J. Neurosci. *18*, 237–250.

Lamprianou, S., Chatzopoulou, E., Thomas, J.L., Bouyain, S., and Harroch, S. (2011). A complex between contactin-1 and the protein tyrosine phosphatase PTPRZ controls the development of oligodendrocyte precursor cells. Proc. Natl. Acad. Sci. USA *108*, 17498–17503.

Lebensohn, A.M., Dubey, R., Neitzel, L.R., Tacchelly-Benites, O., Yang, E., Marceau, C.D., Davis, E.M., Patel, B.B., Bahrami-Nejad, Z., Travaglini, K.J., et al. (2016). Comparative genetic screens in human cells reveal new regulatory mechanisms in WNT signaling. eLife *5*, e21459.

Lebrun-Julien, F., Bachmann, L., Norrmén, C., Trötzmüller, M., Köfeler, H., Rüegg, M.A., Hall, M.N., and Suter, U. (2014). Balanced mTORC1 activity in oligodendrocytes is required for accurate CNS myelination. J. Neurosci. *34*, 8432–8448.

Lee, S., Leach, M.K., Redmond, S.A., Chong, S.Y., Mellon, S.H., Tuck, S.J., Feng, Z.Q., Corey, J.M., and Chan, J.R. (2012). A culture system to study oligodendrocyte myelination processes using engineered nanofibers. Nat. Methods *9*, 917–922.

Lentferink, D.H., Jongsma, J.M., Werkman, I., and Baron, W. (2018). Grey matter OPCs are less mature and less sensitive to IFNγ than white matter OPCs: consequences for remyelination. Sci. Rep. *8*, 2113.

Liu, C., Li, Y., Semenov, M., Han, C., Baeg, G.H., Tan, Y., Zhang, Z., Lin, X., and He, X. (2002). Control of beta-catenin phosphorylation/degradation by a dual-kinase mechanism. Cell *108*, 837–847.

Madhavarao, C.N., Moffett, J.R., Moore, R.A., Viola, R.E., Namboodiri, M.A., and Jacobowitz, D.M. (2004). Immunohistochemical localization of aspartoacylase in the rat central nervous system. J. Comp. Neurol. *472*, 318–329.

Makinodan, M., Rosen, K.M., Ito, S., and Corfas, G. (2012). A critical period for social experience-dependent oligodendrocyte maturation and myelination. Science *337*, 1357–1360.

Matas-Rico, E., van Veen, M., Leyton-Puig, D., van den Berg, J., Koster, J., Kedziora, K.M., Molenaar, B., Weerts, M.J., de Rink, I., Medema, R.H., et al. (2016). Glycerophosphodiesterase GDE2 promotes neuroblastoma differentiation through glypican release and is a marker of clinical outcome. Cancer Cell *30*, 548–562.

Maurel, P., Rauch, U., Flad, M., Margolis, R.K., and Margolis, R.U. (1994). Phosphacan, a chondroitin sulfate proteoglycan of brain that interacts with neurons and neural cell-adhesion molecules, is an extracellular variant of a receptor-type protein tyrosine phosphatase. Proc. Natl. Acad. Sci. USA *91*, 2512–2516.

Mayoral, S.R., and Chan, J.R. (2016). The environment rules: spatiotemporal regulation of oligodendrocyte differentiation. Curr. Opin. Neurobiol. *39*, 47–52.

Mudge, J.M., and Harrow, J. (2015). Creating reference gene annotation for the mouse C57BL6/J genome assembly. Mamm Genome *26*, 366–378.

Munji, R.N., Choe, Y., Li, G., Siegenthaler, J.A., and Pleasure, S.J. (2011). Wnt signaling regulates neuronal differentiation of cortical intermediate progenitors. J. Neurosci. *31*, 1676–1687.

Nave, K.A. (2010). Myelination and support of axonal integrity by glia. Nature *468*, 244–252.

Nogusa, Y., Fujioka, Y., Komatsu, R., Kato, N., and Yanaka, N. (2004). Isolation and characterization of two serpentine membrane proteins containing glycerophosphodiester phosphodiesterase, GDE2 and GDE6. Gene *337*, 173–179.

Park, S., Lee, C., Sabharwal, P., Zhang, M., Meyers, C.L., and Sockanathan, S. (2013). GDE2 promotes neurogenesis by glycosylphosphatidylinositol-anchor cleavage of RECK. Science *339*, 324–328.

Pertea, G. (2010). Fqtrim: trimming and filtering of next-gen reads. http://ccb.jhu.edu/software/fqtrim/.

Power, J., Mayer-Pröschel, M., Smith, J., and Noble, M. (2002). Oligodendrocyte precursor cells from different brain regions express divergent properties consistent with the differing time courses of myelination in these regions. Dev. Biol. *245*, 362–375.

Rao, M., and Sockanathan, S. (2005). Transmembrane protein GDE2 induces motor neuron differentiation in vivo. Science *309*, 2212–2215.

Remahl, S., and Hildebrand, C. (1982). Changing relation between onset of myelination and axon diameter range in developing feline white matter. J. Neurol. Sci. *54*, 33–45.

Rodriguez, M., Choi, J., Park, S., and Sockanathan, S. (2012). Gde2 regulates cortical neuronal identity by controlling the timing of cortical progenitor differentiation. Development *139*, 3870–3879.

Sabharwal, P., Lee, C., Park, S., Rao, M., and Sockanathan, S. (2011). GDE2 regulates subtype-specific motor neuron generation through inhibition of Notch signaling. Neuron *71*, 1058–1070.

Sakane, H., Yamamoto, H., Matsumoto, S., Sato, A., and Kikuchi, A. (2012). Localization of glypican-4 in different membrane microdomains is involved in the regulation of Wnt signaling. J. Cell Sci. *125*, 449–460.

Shevchenko, A., Tomas, H., Havlis, J., Olsen, J.V., and Mann, M. (2006). In-gel digestion for mass spectrometric characterization of proteins and proteomes. Nat. Protoc. *1*, 2856–2860.

Shimogori, T., VanSant, J., Paik, E., and Grove, E.A. (2004). Members of the Wnt, Fz, and Frp gene families expressed in postnatal mouse cerebral cortex. J. Comp. Neurol. *473*, 496–510.

Solly, S.K., Thomas, J.L., Monge, M., Demerens, C., Lubetzki, C., Gardinier, M.V., Matthieu, J.M., and Zalc, B. (1996). Myelin/oligodendrocyte glycoprotein (MOG) expression is associated with myelin deposition. Glia *18*, 39–48.

Spitzer, S.O., Sitnikov, S., Kamen, Y., Evans, K.A., Kronenberg-Versteeg, D., Dietmann, S., de Faria, O., Jr., Agathou, S., and Káradóttir, R.T. (2019). Oligodendrocyte progenitor cells become regionally diverse and heterogeneous with age. Neuron *101*, 459–471.e5.

Stevens, B., Porta, S., Haak, L.L., Gallo, V., and Fields, R.D. (2002). Adenosine: a neuron-glial transmitter promoting myelination in the CNS in response to action potentials. Neuron *36*, 855–868.

Tomassy, G.S., Berger, D.R., Chen, H.H., Kasthuri, N., Hayworth, K.J., Vercelli, A., Seung, H.S., Lichtman, J.W., and Arlotta, P. (2014). Distinct profiles of myelin distribution along single axons of pyramidal neurons in the neocortex. Science *344*, 319–324.

Trapnell, C., Roberts, A., Goff, L., Pertea, G., Kim, D., Kelley, D.R., Pimentel, H., Salzberg, S.L., Rinn, J.L., and Pachter, L. (2012). Differential gene and transcript expression analysis of RNA-seq experiments with TopHat and Cufflinks. Nat. Protoc. *7*, 562–578.

Trapp, B.D., Nishiyama, A., Cheng, D., and Macklin, W. (1997). Differentiation and death of premyelinating oligodendrocytes in developing rodent brain. J. Cell Biol. *137*, 459–468.

Ueda, H., Levine, J.M., Miller, R.H., and Trapp, B.D. (1999). Rat optic nerve oligodendrocytes develop in the absence of viable retinal ganglion cell axons. J. Cell Biol. *146*, 1365–1374.

Umemori, H., Sato, S., Yagi, T., Aizawa, S., and Yamamoto, T. (1994). Initial events of myelination involve Fyn tyrosine kinase signalling. Nature *367*, 572–576.

Wang, S., Sdrulla, A.D., diSibio, G., Bush, G., Nofziger, D., Hicks, C., Weinmaster, G., and Barres, B.A. (1998). Notch receptor activation inhibits oligodendrocyte differentiation. Neuron *21*, 63–75.

Ye, F., Chen, Y., Hoang, T., Montgomery, R.L., Zhao, X.H., Bu, H., Hu, T., Taketo, M.M., van Es, J.H., Clevers, H., et al. (2009). HDAC1 and HDAC2 regulate oligodendrocyte differentiation by disrupting the beta-catenin-TCF interaction. Nat. Neurosci. *12*, 829–838.

Yuan, X., Eisen, A.M., McBain, C.J., and Gallo, V. (1998). A role for glutamate and its receptors in the regulation of oligodendrocyte development in cerebellar tissue slices. Development *125*, 2901–2914.

Zhou, Q., Wang, S., and Anderson, D.J. (2000). Identification of a novel family of oligodendrocyte lineage-specific basic helix-loop-helix transcription factors. Neuron *25*, 331–343.

Zuchero, J.B., Fu, M.M., Sloan, S.A., Ibrahim, A., Olson, A., Zaremba, A., Dugas, J.C., Wienbar, S., Caprariello, A.V., Kantor, C., et al. (2015). CNS myelin wrapping is driven by actin disassembly. Dev. Cell *34*, 152–167.

STAR★METHODS

KEY RESOURCES TABLE

REAGENT or RESOURCE	SOURCE	IDENTIFIER
Antibodies		
Rabbit anti-Olig2	Millipore	Cat# AB9610; RRID:AB_570666
Guinea Pig anti-Olig2	Ben Novitch, University of California Los Angeles	N/A
Mouse anti-NeuN	Millipore	Cat# MAB377; RRID:AB_2298772
Rabbit anti-NeuN	Millipore	Cat# MABN140; RRID:AB_2571567
Rabbit anti-TCF4/TCF7L2	Cell Signaling Technology	Cat# 2569; RRID:AB_2199816
Mouse anti-CC1	Calbiochem	Cat# OP80; RRID:AB_2057371
Rabbit anti-ASPA	Gene Tex	Cat# GTX113389; RRID:AB_2036283
Rabbit anti-Ki67	Abcam	Cat# ab15580; RRID:AB_443209
Goat anti Sox10	Santa Cruz	Cat# Sc-17342; RRID:AB_2195374
Chicken anti-GFP	Aves Labs	Cat# GFP-1020; RRID:AB_10000240
Rabbit anti-GFP	Life Technologies	Cat# A11122; RRID:AB_221569
Sheep Anti-Digoxigenin, POD Conjugated	Roche	Cat# 11207733910; RRID:AB_514500
Mouse anti-MBP	Covance	Cat# SMI-99P-100; RRID:AB_10120129
Rat anti-MBP	Milipore	Cat# MAB386; RRID: AB_94975
Mouse anti-beta-Tubulin III	Sigma-Aldrich	Cat# T8578; RRID:AB_1841228
Rabbit anti-GFAP	Agilent	Cat# Z0334; RRID:AB_10013382
Mouse anti-Active-β-Catenin (Anti-ABC)	Millipore	Cat# 05-665; RRID:AB_309887
Mouse anti-Ran	BD Biosciences	Cat# 610341; RRID: AB_397731
Rabbit anti-Cux1	Proteintech Group	Cat# 11733-1-AP; RRID:AB_2086995
Rat anti-Ctip2	Abcam	Cat# ab18465; RRID:AB_2064130
Mouse anti-MOG	Millipore	Cat# MAB5680; RRID:AB_1587278
Rabbit anti-Neurofilament H	Millipore	Cat# AB1989; RRID:AB_11212727
Rabbit anti-GDE2	This study	N/A
Mouse anti-Actin	Millipore	Cat# MAB1501; RRID:AB_2223041
Rabbit anti-PDGF receptor alpha	Cell Signaling Technology	Cat# 3174; RRID:AB_2162345
Rabbit anti- β-Catenin	Cell Signaling Technology	Cat# 8480; RRID:AB_11127855
Goat anti-Contactin-2/TAG1	R and D Systems	Cat# AF4439; RRID:AB_2044647
Mouse anti-Chondroitin Sulfate Proteoglycan (CAT-315)	Millipore	Cat# MAB1581; RRID:AB_94270
Rabbit anti-GAPDH	Cell Signaling Technology	Cat# 8884; RRID:AB_11129865
Goat anti-rabbit IgG (H+K), secondary antibody, FITC and Alexa 647 conjugates	Jackson ImmunoResearch Labs	Cat# 111-095-144; RRID:AB_2337978, Cat# 111-605-144; RRID:AB_2338078
Goat anti-mouse IgG (H+K), secondary antibody, Cy3 and Alexa 488 conjugates	Jackson ImmunoResearch Labs	Cat# 115-165-146; RRID:AB_2338690, Cat# 115-545-166; RRID:AB_2338852
Goat anti-guinea pig IgG (H+K), secondary antibody, Alexa 647 conjugate	Jackson ImmunoResearch Labs	Cat# 106-605-003; RRID:AB_2337446
Donkey anti-goat IgG (H+L), secondary antibody, Cy3 conjugate	Jackson ImmunoResearch Labs	Cat# 705-165-147; RRID:AB_2307351
Donkey anti-chicken IgY (H+L), secondary antibody, Cy3 conjugate	Jackson ImmunoResearch Labs	Cat# 703-165-155; RRID:AB_2340363
Peroxidase Donkey anti-mouse IgG (H+L), secondary antibody	Jackson ImmunoResearch Labs	Cat# 715-035-150; RRID:AB_2340770
Peroxidase Donkey anti-rabbit IgG (H+L), secondary antibody	Jackson ImmunoResearch Labs	Cat# 711-035-152; RRID:AB_10015282

(*Continued on next page*)

Continued

REAGENT or RESOURCE	SOURCE	IDENTIFIER
Chemicals, Peptides, and Recombinant Proteins		
(Z)-4-Hydroxytamoxifen	Sigma-Aldrich	Cat# H7904
Sunflower seed oil from *Helianthus annuus*	Sigma-Aldrich	Cat# S5007
Neurobasal media	GIBCO	Cat# 21103-049
DMEM/F12 media	GIBCO	Cat# 10565-018
Sodium Pyruvate 100mM	GIBCO	Cat# 11360-070
Glutamax	GIBCO	Cat# 35050-061
N2B supplement	STEMCELL Technologies	Cat# 7156
SM1 supplement	STEMCELL Technologies	Cat# 5711
Penicillin-Streptomycin	GIBCO	Cat# 15140-122
Poly-D-lysine hydrobromide	Sigma-Aldrich	Cat# P0899
Laminin	Sigma-Aldrich	Cat# L2020
PureCol Type I Bovine Collagen Solution	Advanced Biomatrix	Cat# 5005-B
Forskolin	Calbiochem	Cat# 344270
CNTF	PeproTech	Cat# 450-5
HEPES	GIBCO	Cat# 15630080
N-Acetyl-Cysteine	Sigma-Aldrich	Cat# A8199
DAPI	Invitrogen	Cat# R37606
Protease inhibitor cocktail	Sigma-Aldrich	Cat# P8340
Fluo-4, AM	Thermo Fisher Scientific	Cat# F14201
Ionomycin	Tocris	Cat# 1704
Trizol	Thermo Fisher Scientific	Cat# 15596018
Fast SYBR® Green Master Mix	Thermo Fisher Scientific	Cat# 4385612
Alexa Fluor® 488 Phalloidin	Invitrogen	Cat# A12379
Chondroitinase ABC	Sigma-Aldrich	Cat# C3667
Protein L magnetic beads	Thermo Fisher Scientific	Cat# 88849
Bicuculine	Tocris	Cat# 0131
Critical Commercial Assays		
Neural Tissue Dissociation Kit (P)	Miltenyi Biotec	Cat# 130-092-628
Miltenyi Isolation Starting Kit	Miltenyi Biotec	Cat# 130-090-312
Anti-O4 Microbeads	Miltenyi Biotec	Cat# 130-094-543
SuperScript III	Thermo Fisher Scientific	Cat# 18080051
TSA Plus Cy3 system	PerkinElmer	Cat# NEL744001KT
TruSeq® Stranded mRNA LT - Set A	Illumina	Cat# RS-122-2101
RNeasy Plus Micro Kit	QIAGEN	Cat# 74034
NE-PER Nuclear and cytoplasmic extraction reagents	Thermo Fisher Scientific	Cat# 78833
Deposited Data		
RNA-seq data	This study	NCBI's GEO: GSE147144
Mass spectrometry data	This study	ProteomeXchange: PXD018080
Experimental Models: Cell Lines		
Primary cortical oligodendrocyte progenitor cells	This study	N/A
Primary cortical neuronal cells	This study	N/A
Experimental Models: Organisms/Strains		
Mouse: *Gde2KO*	Sabharwal et al., 2011	N/A
Mouse: *Gde2^{flox}*	Sabharwal et al., 2011	N/A
Mouse: *PdgfrαCre-ER*	Kang et al., 2010	N/A

(*Continued on next page*)

Continued

REAGENT or RESOURCE	SOURCE	IDENTIFIER
Mouse: *Nex-Cre*	Goebbels et al., 2006	N/A
Mouse: *Rosa26 Tcf./Lef H2B-EGFP*	Cho et al., 2017	N/A
Mouse: *Ctnnb1*^{flex3}	Harada et al., 1999	N/A
Oligonucleotides		
Gde2 PCR primers Forward: 5′ CAGAAGGGACCAAGCACTCA 3′	Sabharwal et al., 2011	N/A
Gde2 PCR primers: Reverse: 5′ CCCGTTGGTTGACATTCGTG 3′	Sabharwal et al., 2011	N/A
Gde2 in situ hybridization primers: Forward: 5′ CCTCAAGACCGACCCCTT 3′	Allen brain atlas	http://mouse.brain-map.org/
Gde2 in situ hybridization primers: Reverse: 5′ GGGGCATGATCCAGAGTG 3′	Allen brain atlas	http://mouse.brain-map.org/
Mbp in situ hybridization primers: Forward: 5′ GAGGCCTGGATGTGATGG 3′	Allen brain atlas	http://mouse.brain-map.org/
Mbp in situ hybridization primers: Reverse: 5′ GGGGAACAAGTCAGGGCT 3′	Allen brain atlas	http://mouse.brain-map.org/
Gde2 qPCR primers Forward: 5′ GGCTCCAGAACACACAGTGA 3′	This study	N/A
Gde2 qPCR primers Reverse: 5′ CAGGACAGTCCAGTTGAGCA 3′	This study	N/A
Lef1 qPCR primers: Forward: 5′ ATGCACGTGAAGCCTCAACA 3′	Elbaz et al., 2016	N/A
Lef1 qPCR primers: Reverse: 5′ AGCTGCACTCTCCTTTAGCG 3′	Elbaz et al., 2016	N/A
Gapdh qPCR primers: Forward: 5′ CGTCCCGTAGACAAAATGGT 3′	Lebrun-Julien et al., 2014	N/A
Gapdh qPCR primers: Reverse: 5′ TTGATGGCAACAATCTCCAC 3′	Lebrun-Julien et al., 2014	N/A
Software and Algorithms		
ImageJ/Fiji version 1.52d	National Institutes of Health	https://imagej.nih.gov/ij/index.html
Corel Draw X8	Corel	http://www.corel.com/en/
Adobe Photoshop CC 2017	Adobe	https://www.adobe.com
GraphPad Prism 5	GraphPad	https://www.graphpad.com/
Imaris	BITPLANE	https://imaris.oxinst.com
FastQC	Babraham Bioinformatics	https://www.bioinformatics.babraham.ac.uk/projects/fastqc/
Fqtrim	Johns Hopkins University	https://ccb.jhu.edu/software/fqtrim/
Tophat2 v2.1.1	Johns Hopkins University	https://ccb.jhu.edu/software/tophat/index.shtml
Cufflinks v2.2.1	Cole Trapnell, University of Washington	http://cole-trapnell-lab.github.io/cufflinks/
Mouse UniProt protein database (released on May 2018)	Uniprot Consortium	https://www.uniprot.org/
MaxQuant v1.5.5.1	Cox and Mann, 2008	https://www.biochem.mpg.de/5111795/maxquant

RESOURCE AVAILABILITY

Lead Contact

Further information and requests for reagents should be directed to and will be fulfilled by the Lead Contact, Shanthini Sockanathan (ssockan1@jhmi.edu).

Materials Availability

Antibodies against mouse GDE2 will be provided freely with no restrictions by the Lead Contact upon request.

Data and Code Availability

The RNA-seq raw data generated during this study are publicly available at National Center for Biotechnology Information (NCBI) Gene Expression Omnibus (GEO). The accession number for the data reported in this paper is GSE147144.

The mass spectrometry proteomics data have been deposited to the ProteomeXchange Consortium (http://proteomecentral.proteomexchange.org) via the PRIDE partner repository with the dataset identifier PXD018080.

EXPERIMENTAL MODEL AND SUBJECT DETAILS

Mice

The following mouse lines were used in this study: *Gde2KO* (Sabharwal et al., 2011), *Gde2*^{flox} (Sabharwal et al., 2011), *Pdgfr*α*Cre-ER* (Kang et al., 2010), *Nex-Cre* (Goebbels et al., 2006), *Rosa26 Tcf./Lef H2B-EGFP* (Cho et al., 2017), *Ctnnb1*^{flex3} (Harada et al., 1999). All mice were housed and handled according to the approved Institutional Animal Care and Use Committee (IACUC) protocol of the Johns Hopkins Medical Institution. Both males and females were used for analysis. The age of the animals analyzed are stated in the figures, figure legends and main text.

METHOD DETAILS

Tissue processing and immunohistochemistry

Mice were deeply anesthetized with Avertin solution (1.3% 2,2,2-Tribromorethanol (Fluka 90710) and 0.7% 2-methyl-2-butanol (Sigma 240486) in Phosphate Buffered Saline (PBS) at 0.02 ml/g body weight and perfused transcardially with 0.1 M Phosphate Buffer (PB) followed by fixation solution (4% paraformaldehyde in 0.1 M PB). The brains were postfixed in the fixation solution overnight at 4°C and transferred to 30% sucrose solution and stored at 4°C for more than 48 hr. The tissues were embedded in O.C.T. Compound (Tissue-Tek 62550–12), flash frozen, and coronally sectioned (50 μm for P7 brain tissues and 35 μm for the rest) with a cryostat (Thermo Fisher Scientific HM550). Immunofluorescence was performed on free-floating sections. Brain sections were boiled in sodium citrate buffer (10 mM sodium citrate with 0.05% Tween-20) at 95°C before blocking. Tissue sections were pre-incubated in blocking solution (1% normal goat serum, 0.3% Triton X-100 in PBS) for 2 hours at room temperature, then incubated in primary antibodies overnight at 4°C. The primary antibodies and secondary antibodies used are listed in the Key Resources Table. Sections were mounted onto slides with mounting reagent (Polysciences 18606). Images were acquired using confocal microscopy (Zeiss LSM700) with 10 or 20x objective. A total of 4-5 sections were assessed per mouse and 3-5 mice were analyzed per group. For all studies, a region of interest (ROI) was chosen based on the anatomical structures of CC and CTX based on DAPI staining, subsequent to quantification (see section on Quantification and Statistical Analyses).

4-HT preparation and administration

4-hydroxytamoxifen (4-HT, sigma H7904) was prepared as described previously (Badea et al., 2003). 0.2 mg of 4HT was injected to P7 pups intraperitoneally. Pups were sacrificed to collect tissue samples at P11.

Fluorescent *in situ* hybridization (FISH)

Embedded frozen tissues were sectioned at 16 μm. Sections were incubated in 3% hydrogen peroxide to block endogenous peroxidase activity and permeabilized with 0.3% Triton X-100 in PBS. Sections were acetylated in 0.3% acetic anhydride. After pre-hybridization, slides were hybridized with digoxigenin-labeled sense and antisense probes overnight at 65°C. Primers used to generate probes against *Gde2* and *Mbp* are listed in the Key Resources Table. To couple FISH with immunohistochemistry, sections were blocked in blocking solution (PerkinElmer FP1020) and incubated with sheep anti-digoxigenin-POD, 1:500 (Roche 11207733910) and relevant primary antibodies overnight at 4°C. After incubation with secondary antibodies (1 hour, room temperature), fluorescent signals were developed with TSA Plus Cy3 system (PerkinElmer NEL744001KT) according to the manufacturer's instructions. Images were acquired on a confocal microscope (Zeiss LSM700) with 20x objective and on Zeiss LSM800 with 10x objective for tiling (9x9).

Transmission Electron Microscopy (TEM)

Anesthetized mice were perfused intracardially with fixative containing 2% PFA (EM grade), 2% glutaraldehyde, 50 mM PO4, 5 mM MgCl2, in 50mM sodium cacodylate buffer, pH 7.4, for 30 min at a rate of 1 ml/min for P14 and 2min/ml for 10-week-old mice. Brains were post-fixed in the same fixative overnight at 4°C. CC and adjacent CTX containing the ROI were carefully dissected out from 1000 μm coronally sectioned brain slices. For TEM imaging and analysis of the CC, the sagittal surface near the midline of the CC was sectioned further. All tissues were serially dehydrated, embedded, and sectioned by the JHU SOM Microscope Facility as previously described (Baxi et al., 2015). Images were acquired with a Hitachi 7600 TEM. Images (under 9700x and 65000x magnification) were obtained from the CC below the CTX at random with the operator blinded. ImageJ (National Institutes

of Health) software was used to measure the number of myelinated axons and g-ratio per unit area. For g-ratio analysis, the diameters of axons and outer myelinated axons were calculated from the surface area derived from the circumference of each. For g-ratio analysis of P11 samples, selection of myelinated axons was unbiased. Specifically, a grid was first created, and axons located at grid line intersections were selected for g-ratio analysis. 100 myelinated axons were counted from 10∼13 ROIs (under 9700x magnification) per animal and three animals were used per condition. For myelin sheath analysis of 10 week old samples, more than 500 axons with diameter greater than 0.5 μm were counted from 6∼9 ROIs (under 9700x magnification) per animal with three animals per condition.

Cell culture

Mouse primary cortical neuronal cultures were prepared from embryonic day 16.5 (E16.5) fetuses from timed-pregnant mice using Neural Tissue Dissociation Kits (Miltenyi Biotec 130-092-628) according to the manufacturer's recommendations. Cortical preparations were plated at a density of 2.5×10^5 cells per cm^2 on plastic wells (6-well plate) or glass coverslips coated with poly-D-lysine (0.1 mg/ml in 0.1 M Trizma buffer pH 8.5) containing 1% laminin (Sigma-Aldrich L2020) and 1% PureCol Type I Bovine Collagen Solution (Advanced Biomatrix 5005-B). Cells were initially cultured in neurobasal medium (GIBCO 21103-049) containing 5% fetal horse serum, 1% penicillin/streptomycin (GIBCO 15140122), 1% Glutamax-I (GIBCO 35050061), 1% sodium pyruvate (GIBCO 11360070), 30 mM Glucose, and 2% SM1 supplement (STEMCELL Technologies 5711). The next day on DIV1, the medium was replaced with Neurobasal medium with 1% penicillin/streptomycin, 1% Glutamax-I, 1% sodium pyruvate, 30 mM Glucose, 2% SM1 supplement, and 1% N2B (STEMCELL Technologies 7156). OPCs were obtained from P6 cortices of WT pups using Neural Tissue Dissociation and Isolation kits (Miltenyi Biotec 130-090-312) with magnetic beads (Miltenyi Biotec 130-094-543) to positively select O4+ cells according to the manufacturer's recommendations. For neuron-OL cocultures, freshly isolated OPCs in coculture media (half DMEM:F12 and half Neural basal media containing 10 mM HEPES (GIBCO 15630080), 2% SM1 supplement, 1% N2B, 0.5% penicillin/streptomycin, 5 μg/mL N-Acetyl-Cysteine (Sigma A8199), 5 μM Forskolin (Calbiochem 344270), 10ng/mL CNTF (PeproTech 450-50) were added at a density of 30,000 cells on top of DIV3 neurons and cocultured for indicated time periods. Neuronally conditioned media (CM) were collected from neuronal cultures on DIV3 and spun at 3,000xg for 10 minutes at 4°C to remove cellular debris. Freshly isolated WT OPCs in DIV3 CM were plated at a density of 15,000 cells per cm^2 on plastic wells (24-well plate) or glass coverslips coated with poly-D-lysine (0.1 mg/ml in distilled water) containing 1% laminin. One day after plating, cells were replenished with CM collected from neurons on DIV4 and cultured for another 2 days prior to further analyses. For depletion of phosphacan from CM, CAT-315 antibodies recognizing neuronal phosphacan were bound to protein L magnetic beads (Thermo Fisher Scientific 88849). Antibody-bound protein L magnetic beads were subsequently incubated with WT CM overnight at 4°C.

Immunocytochemistry

Cultured cells were fixed with 4% PFA solution for 10 minutes and permeabilized in PBS with 0.3% Tween-20 for 10 minutes followed by blocking with PBS containing 1% bovine serum albumin (BSA) and 0.15% Tween-20 for 1 hour at room temperature. The cells were incubated with primary antibodies diluted in PBS (1:500) overnight at 4°C. Primary antibodies used were as follows: Rat anti-MBP (Millipore MAB386), rabbit anti-Olig2 (Millipore AB9610), guinea pig anti-Olig2 (from B. Novitch), mouse anti-MBP (Covance SMI-99P-100), mouse anti-beta-Tubulin III (Sigma-Aldrich T8578), Rabbit anti-Neurofilament H (Millipore AB1989), rabbit anti-GFAP (Agilent Z0334), mouse anti-Active-β-Catenin (Anti-ABC) (Millipore 05-665). After incubation with appropriate secondary antibodies (1 hour room temperature), cells were counterstained with DAPI (Invitrogen R37606). To visualize F-actin network, cells were stained with Alexa Fluor 488-phalloidin (Invitrogen A12379) during secondary antibody incubation. Cells were mounted on slides with mounting reagent and imaged using confocal microscope (Zeiss LSM700) with 20x objective and on epifluorescence microscope (Keyence BZ-X710) with 10x objective for tiling (3x3).

Calcium transient imaging and analysis

Cortical neurons were loaded with the synthetic calcium indicator Fluo-4, AM (Thermo Scientific F14201) on DIV3. 4 mM Fluo-4 stock solution in DMSO (Sigma D8418) was diluted in HEPES-buffered extracellular solution (143 mM NaCl, 5 mM KCl, 2 mM CaCl2, 1 mM MgCl2, 10 mM HEPES, 10 mM glucose, pH 7.2, osmolality 305-310 mOsm) to yield 2 μM working solution. At the end of image acquisition, 2 μM ionomycin (Tocris 1704) was added into each well as a positive control. Live recorded images of spontaneous calcium activity were acquired with epifluorescence microscope (Keyence BZ-X710) under 10X objective. Images were streamed at 3 Hz frame rate for 3.5 minutes. Each image frame was 680 × 480 pixels, which corresponded to 0.32 mm^2 rectangular area. F_0 (baseline) and F are the mean fluorescence intensities and fluorescence intensities at a given time in each ROI, respectively. A change in fluorescence (Δ F/F0) was considered as a Ca^{2+} rise if it was > 10%. For peak analysis, F_0 for each ROI trace was manually adjusted to zero. Each data point represents mean value of $\Delta F/F_0$ from at least 11 recordings per group at a given time.

mRNA-sequencing analysis

RNA-seq studies were performed using 5 week WT and *Gde2KO* spinal cords. The ventral half of the lumbar spinal cord was freshly dissected from 3 WT and 3 *Gde2KO* animals, and poly-adenylated mRNA was extracted using a QIAGEN RNeasy Plus Mini Kit (QIAGEN, 74134). cDNA libraries were prepared using the Illumina TruSeq Stranded mRNA Library Prep Kit (Illumina, RS-122-2101). Paired-end reads, 50 bp in length, were generated on an Illumina HiSeq 2500 system yielding between 50-61 million reads

per sample. To analyze the RNA-seq data, reads were quality checked and trimmed using the programs fastqc (Andrews, 2010) and fqtrim (Pertea, 2010). Reads were then mapped to the mouse genome mm10 using the spliced alignment program Tophat2 v2.1.1 (Kim et al., 2013) and assembled into transcripts using Cufflinks v2.2.1 (Trapnell et al., 2012). Mapping rates ranged from 91.7% to 95.2%, with 83%–88% representing exonic reads, indicating very high-quality sequences. Transcript assemblies across all samples were merged with Cuffcompare v.2.2.1, using GENCODE v.M5 (https://www.gencodegenes.org/) (Mudge and Harrow, 2015) as reference, to create a set of gene and transcript annotations that was later used in the differential analyses. Lastly, Cuffdiff v2.2.1 was run on each pairwise comparison to determine statistically significant differentially expressed genes (cutoffs: p-val $\leq$ 0.05).

Mass spectrometry analysis

Neuronal CM samples were subjected to SDS-PAGE, followed by in-gel trypsin digestion (Shevchenko et al., 2006). The extracted peptides were analyzed on an Orbitrap Fusion Lumos Tribrid Mass Spectrometer coupled with the UltiMate 3000 RSLCnano liquid chromatography system (Thermo Fisher Scientific). The peptides were loaded on Acclaim PepMap100 Nano-Trap Column (100 μm × 2 cm, Thermo Fisher Scientific). Peptides were resolved at 300-nl/min flow rate using a linear gradient of 10% to 35% solvent B (0.1% formic acid in 95% acetonitrile) over 95 minutes on an EASY-Spray column (50 cm x 75 μm ID, Thermo Fisher Scientific). MaxQuant (v1.5.5.1) software was used for quantitation and identification of proteins from the mass spectrometry data using mouse UniProt database (released on May 2018) with common contaminant proteins (Cox and Mann, 2008). Search parameters included, a) trypsin as a proteolytic enzyme with up to 2 missed cleavages; b) first search peptide mass error tolerance of 20 ppm and the main search peptide mass error tolerance of 4 ppm; c) fragment mass error tolerance of 20 ppm; d) carbamidomethylation of cysteine (+57.02146 Da) as a fixed modification: e) oxidation of methionine (+15.99492 Da) and protein acetyl (+42.01056 Da) on N terminus as dynamic modifications. Peptides and proteins were filtered at 1% false-discovery rate.

Immunoblotting

Samples were sonicated in lysis buffer (20 mM Tris-HCl pH 8.0, 130 mM NaCl, 2 mM EDTA, 0.5% Triton X-100, 0.5% NP-40, and 0.2% sodium deoxycholate) containing protease inhibitor cocktail (Sigma-Aldrich P8340), subjected to reducing SDS-PAGE, and transferred to PVDF membranes for immunoblotting. For detection of phosphacan in CM, CM samples were equilibrated at a final concentration of 3 mg/ml in chondroitinase buffer (50 mM Trizma, 60 mM sodium acetate, pH 8.0) and treated with chondroitinase ABC (0.25 U per 200 μg protein) from Proteus Vulgaris (Sigma-Aldrich, C3667) for 8 hours at 37°C. CM samples were then boiled in 1x gel loading buffer for electrophoresis and immunoblotting. Nuclear and cytosolic fractions were isolated by Nu-PER Nuclear and Cytoplasmic Extraction Reagents (Thermo Fisher Scientific 78833) according to the manufacturer's instructions. Transferred membranes were incubated with primary antibodies overnight at 4°C. Primary antibodies used were as follows: Rabbit anti-Olig2 (1:2,000 Millipore AB9610), Mouse anti-MBP (1:2,000 Covance SMI-99P-100), Mouse anti-MOG (1:3,000 Millipore MAB5680), Rabbit anti-Neurofilament H (1:10,000 Millipore AB1989), Rabbit anti-GDE2 (1:1000), Rabbit anti-PDGF receptor alpha (1:2,000 Cell Signaling Technology 3174), rabbit anti-Olig2 (Millipore AB9610), Mouse anti-ABC (1:1,000 Millipore 05-665), Ran (10,000 BD Biosciences 610341), Rabbit anti-β-Catenin (1:2,000 Cell Signaling Technology 8480), Goat anti-Contactin-2/TAG1 (1:1000 R and D Systems AF4439), Mouse anti-Chondroitin Sulfate Proteoglycan (CAT-315) (1:5000 Millipore MAB1581), Rabbit anti-GAPDH (1:1,000 Cell Signaling Technology 8884), Mouse anti-Actin (1:10,000 Millipore MAB1501). After incubation with appropriate HRP-conjugated secondary antibodies (1 hour room temperature), membranes were developed by film or by using a digital imaging system (KwikQuant, Kindle Biosciences).

Quantitative real-time PCR

Total RNA from *in vivo* or *in vitro* samples was extracted using Trizol (Thermo Fisher Scientific 15596018) and reverse transcription was carried out using SuperScript III (Thermo Fisher Scientific 18080051) according to the manufacturer's instructions. SYBR-green labeling (Thermo Fisher 4385612) was used for quantitative real-time PCR (Applied Biosystems). The Comparative CT (ΔΔCt) method was used to determine the relative quantities of mRNA. The primers used are listed in the Key Resources Table.

QUANTIFICATION AND STATISTICAL ANALYSIS

3D Image quantification was performed using semi-automated Imaris (Bitplane). For quantification, 4-5 sections per animal and 3-5 animals per group were used. Littermate controls were utilized throughout the study. Images were obtained from brain regions of CC and CTX corresponding to retrosplenial and motor areas. After 3D image reconstruction, each ROI (CC and CTX) was created using the contour function in Imaris. Using spot and surface detection functions, parameters were set for size and fluorescent signal intensity threshold to create an object representing a nucleus or a cell body. After manual validation of parameter settings, the entire z stack was subjected to automated quantification using Imaris. Then, false-positive and false negative spots and surfaces were manually corrected. Number of cells was normalized to surface area of each ROI. All studies were blinded to the investigator. For quantifying intensity of *Gde2* transcript signal in FISH, mean signal intensity of *Gde2* channel (TSA-cy3) within each created 3D object (Olig2+ or NeuN+ cells) was obtained using Imaris. Percent cells expressing *Gde2* and mean intensity of *Gde2* signal per cell were analyzed. For quantifying GFP^+ nuclei in *Rosa26 Tcf./Lef-H2B-EGFP* mice, spots were designated

as GFP^+ when above a set threshold signal intensity. This threshold was applied across all analysis. The number of $NeuN^+$ GFP^+ and $Olig2^+$ GFP^+ cells in each ROI was analyzed using MATLAB modules in Imaris. For quantifying MBP^+ OLs at Stage1-Stage3 in culture, 3x3 tiled images with 10x objective (3.99 mm^2 area) were acquired from 2 wells per animal with at least three biological samples per experiment. The number of MBP^+ cells for each stage was divided by the number of Olig2+ cells in each group and then normalized to control. GraphPad Prism 5 software was used to generate plots and to conduct statistical analysis. The mean ± SEM are shown. Statistical significance was determined by a two-tailed, unpaired Student's t test, 1-way or 2-way ANOVA test and is shown by * $p < 0.05$, ** $p < 0.01$, *** $p < 0.001$. Power analysis (Sample Size Calculator, provided by UCSF Clinical & Translational Science Institute; https://www.sample-size.net/sample-size-means/) was conducted for all analyses. All samples sizes are sufficient to reach 80% power that detect estimated difference in means with a 5% significance level.

Cell Reports, Volume *31*

Supplemental Information

GDE2-Dependent Activation of Canonical Wnt Signaling in Neurons Regulates Oligodendrocyte Maturation

Bo-Ran Choi, Clinton Cave, Chan Hyun Na, and Shanthini Sockanathan

Figure S1

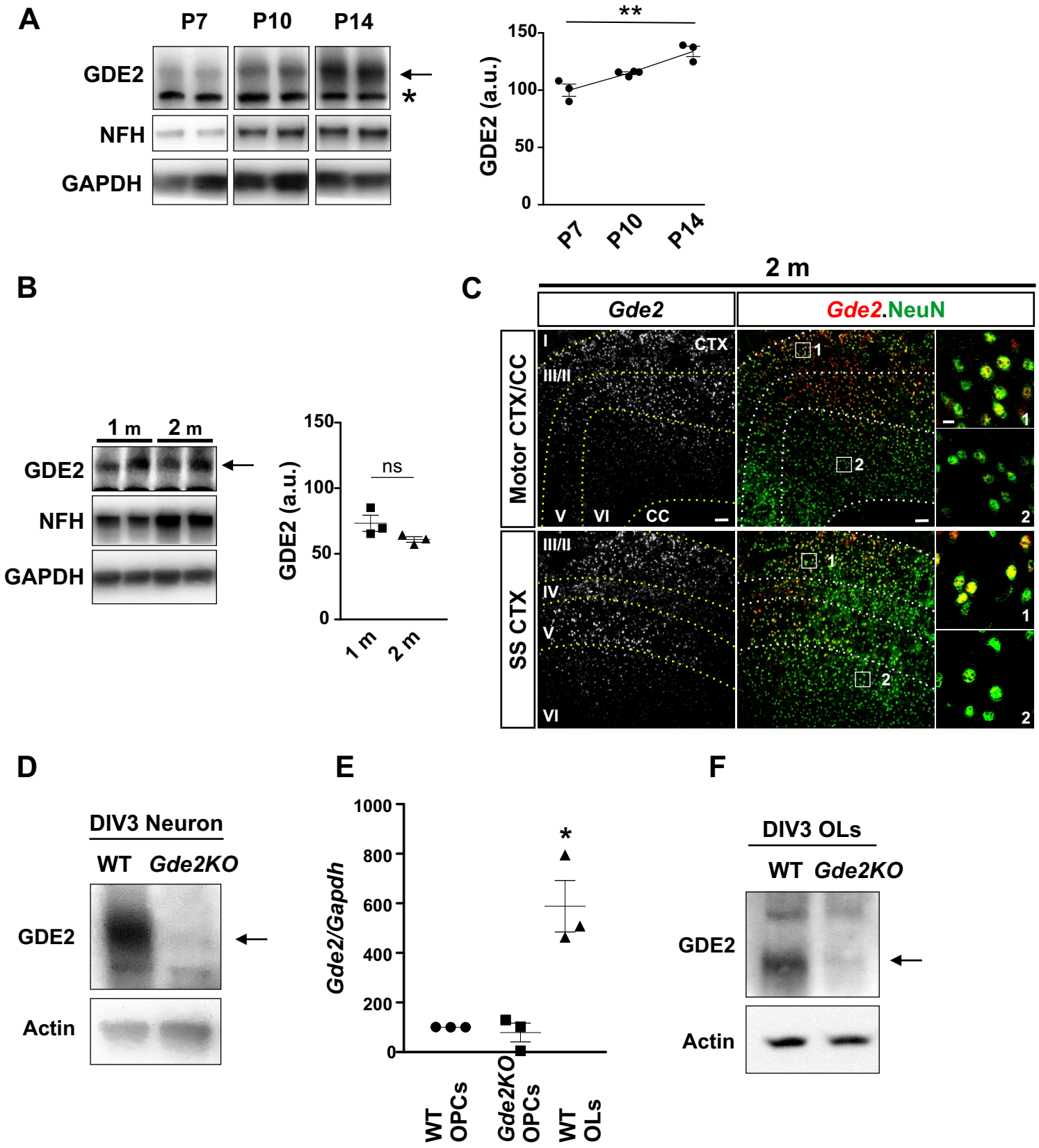
A
P7
P10
P14
GDE2
NFH
GAPDH
*
**
GDE2 (a.u.)
150
100
50
0
P7
P10
P14
B
1 m
2 m
GDE2
NFH
GAPDH
ns
GDE2 (a.u.)
150
100
50
0
1 m
2 m
C
2 m
Gde2
Gde2.NeuN
Motor CTX/CC
SS CTX
I
III/II
CTX
V
VI
CC
IV
1
2
D
DIV3 Neuron
WT
Gde2KO
GDE2
Actin
E
Gde2/Gapdh
1000
800
600
400
200
0
*
WT OPCs
Gde2KO OPCs
WT OLs
F
DIV3 OLs
WT
Gde2KO
GDE2
Actin

Figure S1. Related to Figure 1. GDE2 is expressed in neurons and OLs.

(A) Western blot of cortical extracts from WT animals at postnatal day 7 (P7), P10 and P14. GAPDH is a loading control, NFH is expressed in axons and provides a readout of neurons in brain tissue. Arrow indicates GDE2. Asterisk indicates a nonspecific band. Graph quantifying Western data from P7-P14. a.u. = arbitrary units. **p = 0.0013. n = 3 P7, 4 P10, 3 P14, 1-way ANOVA. (B) Western blot and quantification of GDE2 protein expression at 1 and 2 months (m) of age. ns p = 0.182. n = 3 for each timepoint, two-tailed unpaired t-test. (C) Cortical coronal sections showing *Gde2* transcript distribution. CC: corpus callosum, SS: somatosensory cortex. Cortical layers are marked by dotted lines. Boxed areas 1 and 2 are magnified in right panels. Scale bar: 100 μm, insets 10 μm (D) Western blot of DIV3 cortical neuronal cultures. Arrow marks GDE2. Actin is a loading control. (E) qPCR of *Gde2* transcripts normalized to *Gapdh* mRNA. *p = 0.0021. n = 3 sets of WT, *Gde2KO* OPCs, and WT OLs, 1-way ANOVA. (F) Western blot shows GDE2 is expressed in WT OLs (marked by arrow). Actin is a loading control. All graphs: Mean ± sem.

Figure S2

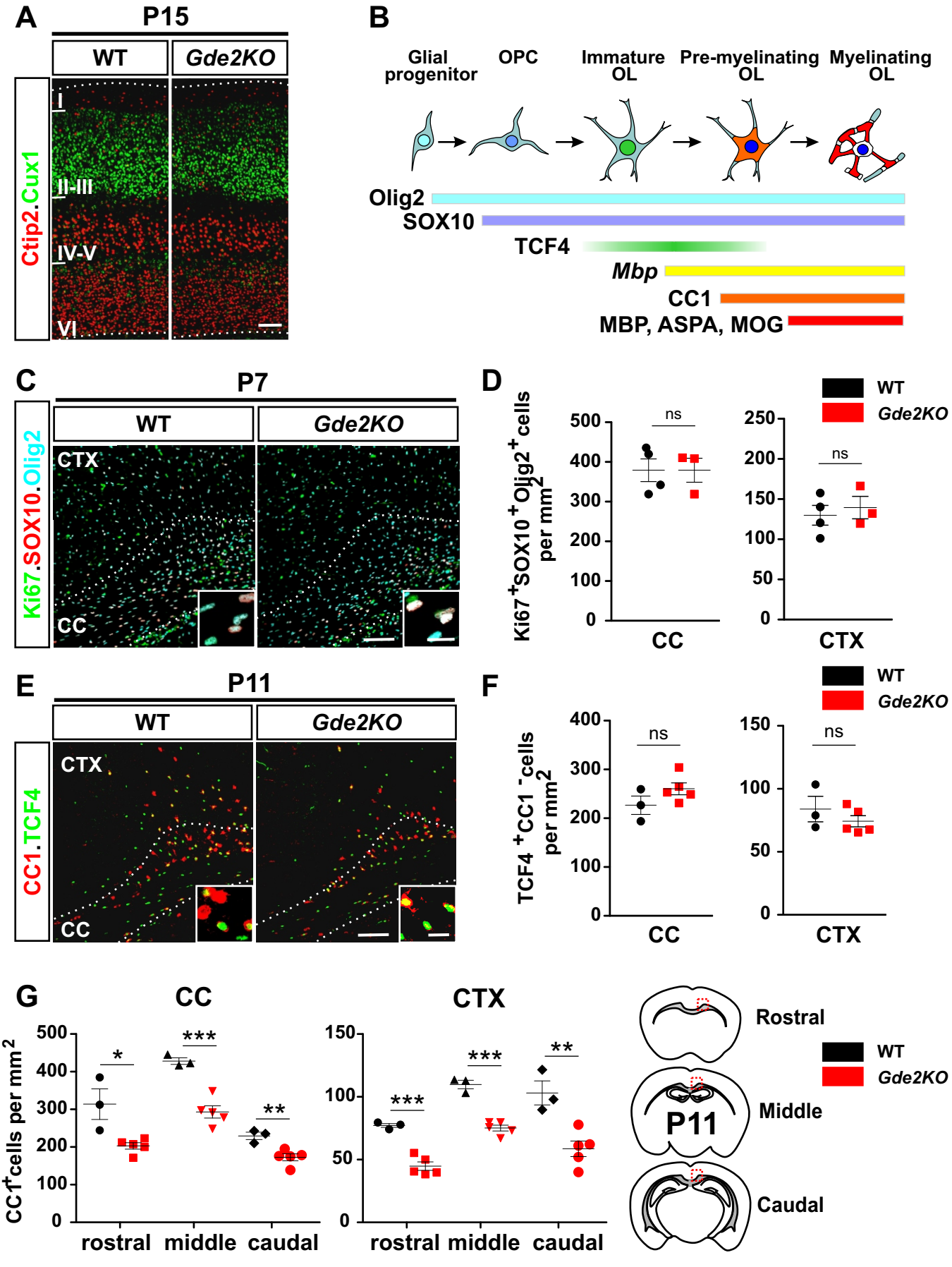
A
P15
WT
Gde2KO
Ctip2.Cux1
I
II-III
IV-V
VI
B
Glial progenitor
OPC
Immature OL
Pre-myelinating OL
Myelinating OL
Olig2
SOX10
TCF4
Mbp
CC1
MBP, ASPA, MOG
C
P7
WT
Gde2KO
Ki67.SOX10.Olig2
CTX
CC
D
Ki67+SOX10+Olig2+ cells per mm2
WT
Gde2KO
ns
CC
CTX
E
P11
WT
Gde2KO
CC1.TCF4
CTX
CC
F
TCF4+CC1- cells per mm2
WT
Gde2KO
ns
CC
CTX
G
CC
CTX
CC1+cells per mm2
rostral
middle
caudal
*
**
***
Rostral
Middle
Caudal
P11
WT
Gde2KO

Figure S2. Related to Figure 2. GDE2 loss impairs OL maturation.

(A) Coronal section of P15 mouse cortex, hatched lines mark cortical boundaries. Cortical layers I-VI are marked. (B) Schematic showing the progression of OL maturation coincident with marker expression. (C) Coronal section of P7 mouse cortex (CTX) and corpus callosum (CC). Hatched line marks boundary between CTX and CC. Inset box shows magnified image of proliferating OPCs (white, Ki67+Sox10+Olig2+). (D) Graphs quantifying the number of proliferating OPCs (Ki67+Sox10+Olig2+) CC ns p = 0.9981 and CTX ns p = 0.6352, n = 4 WT, 3 *Gde2KO*. Two tailed unpaired Student's t-test. (E) Coronal section of P11 mouse CTX and CC. Hatched line demarcates the CC. Inset box shows magnified image of immature (TCF4+CC1-) and mature OLs (CC1+). (F) Graphs quantifying the number of immature OLs (TCF4+CC1-). CC ns p = 0.2306 and CTX ns p = 0.8021, n = 3 WT, 5 *Gde2KO*. Two tailed unpaired Student's t-test. (G) Graphs quantifying number of CC1+ cells in boxed areas in rostral, middle and caudal regions of mouse P11 CC and CTX as shown in schematic. Data for middle regions are the same as in Figure 2B and are reproduced here for comparison purposes. CC: *p rostral = 0.013 ***p middle = 0.0007 **p caudal = 0.0072; CTX: *p rostral = 0.0004 ***p middle = 0.0035 **p caudal = 0.0063. n = 3 WT 5 *Gde2KO*. Two tailed unpaired Student's t-test. All graphs: Mean ± sem. Scale bars: (A, C, E) 100 μm, insets (C, E) 5 μm.

Figure S3

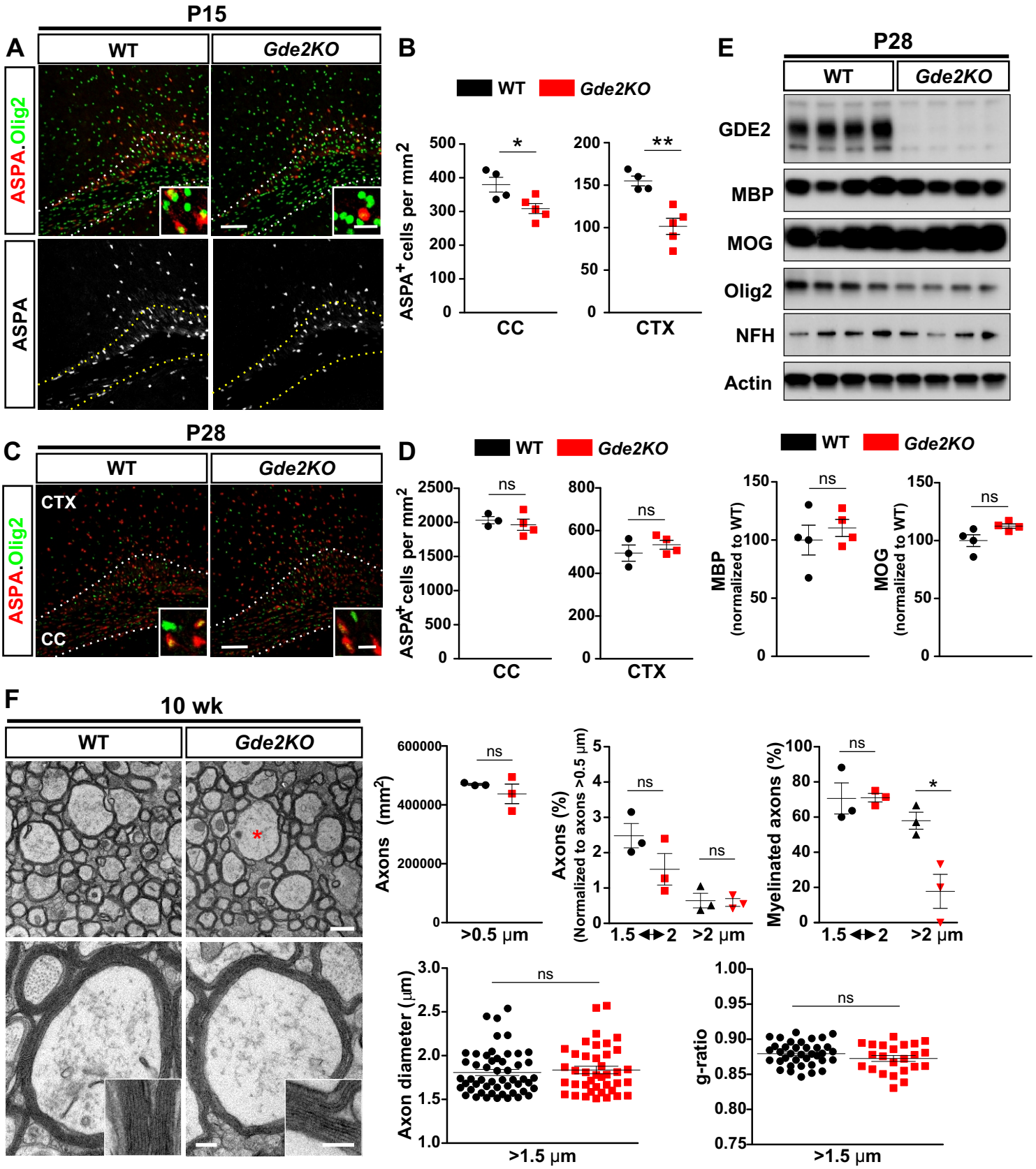
P15
A
WT
Gde2KO
ASPA.Olig2
ASPA
B
WT
Gde2KO
ASPA+cells per mm2
CC
CTX
E
P28
GDE2
MBP
MOG
Olig2
NFH
Actin
C
P28
CTX
CC
D
ns
MBP (normalized to WT)
MOG (normalized to WT)
F
10 wk
Axons (mm2)
>0.5 µm
Axons (%) (Normalized to axons >0.5 µm)
1.5◄►2
>2 µm
Myelinated axons (%)
Axon diameter (µm)
>1.5 µm
g-ratio

Figure S3. Related to Figure 2. *Gde2* KOs show recovery of myelin protein but have decreased myelination of large-diameter axons.

(A, C) Coronal sections of mouse cortex (CTX) and corpus callosum (CC). Hatched lines delineate the CC. Insets show high magnification of mature OLs. Scale bars: 100 μm insets: 10 μm in A and C. (B, D) Graphs quantifying numbers of ASPA+ OLs in CC and CTX. (B) CC *p = 0.0275 and CTX **p = 0.0028, n = 4 WT, 5 *Gde2KO* (D) CC ns p = 0.539 and CTX ns p = 0.4373, n = 3 WT, 4 *Gde2KO*. (E) Western blot of cortical extracts from P28 animals. Graphs quantifying myelin associated proteins MBP ns p = 0.5198, MOG ns p = 0.1035 n = 4 WT, 4 *Gde2KO.* (F) Representative TEM images of 10 week WT and *Gde2KO* animals. * marks exemplar unmyelinated larger-diameter axon in *Gde2KO* condition. Scale bar: (Top) 1 μm, (Bottom) 200 nm, Inset 100 nm. Graphs quantifying axon numbers (ns p = 0.3905) and the percentage of axons with diameters between 1.5 and 2μm (ns p = 0.1649) and larger than 2μm (ns p = 0.8323). Although the percentage of myelinated axons between 1.5 and 2μm is equivalent between WT and *Gde2KO* animals (ns p = 0.9667), the percentage of myelinated axons with diameters larger than 2μm is dramatically reduced (*p = 0.0206) n = 3 WT, 3 *Gde2KO.* Diameters of axons greater than 0.5μm (ns p = 0.5977) and g-ratios of myelinated axons with diameters larger than 1.5μm are unchanged between WT and *Gde2KO* animals (ns p = 0.156). Each point refers to individual myelinated axons from 3 WT and 3 *Gde2KO*. All graphs Mean ± sem, two tailed unpaired t-test.

Figure S4

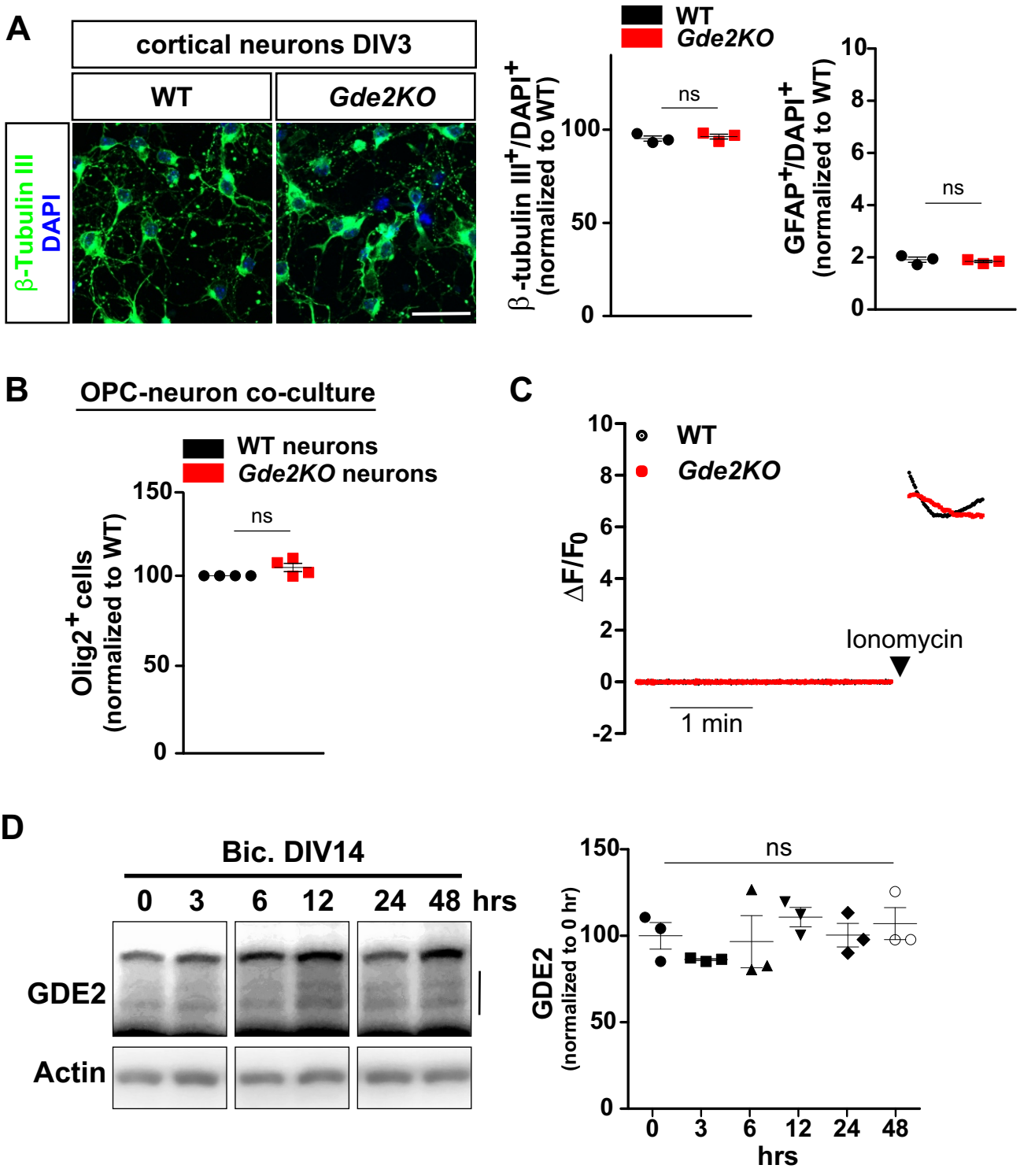
A
cortical neurons DIV3
WT
Gde2KO
β-Tubulin III
DAPI
WT
Gde2KO
ns
β-tubulin III+/DAPI+ (normalized to WT)
GFAP+/DAPI+ (normalized to WT)
B
OPC-neuron co-culture
WT neurons
Gde2KO neurons
ns
Olig2+ cells (normalized to WT)
C
WT
Gde2KO
ΔF/F0
Ionomycin
1 min
D
Bic. DIV14
0 3 6 12 24 48 hrs
GDE2
Actin
ns
GDE2 (normalized to 0 hr)
hrs

Figure S4. Related to Figure 4. Characterization of neuron-OPC co-cultures.

(A) Immunocytochemical staining of DIV3 cortical neuronal cultures. Scale bar: 50 μm. Graphs quantifying percentage neurons (β-tubulin III+) and astrocytes in DIV3 WT and *Gde2KO* cortical neuronal cultures (β-tubulin III+ ns p = 0.6243; GFAP+ ns p = 0.6093; n = 3 WT 3 *Gde2KO*). (B) Graph quantifying the number of Olig2+ cells after neuron-OPC co-culture (ns p = 0.1235, n = 4 WT neuron-WT OPC co-cultures, 4 *Gde2KO* neuron-WT OPC co-cultures). Two tailed unpaired Student's t-test. All graphs: Mean ± sem. (C) Graph of fluorescence changes (Δ F/F0) in DIV3 WT and *Gde2KO* neurons loaded with the calcium indicator Fluo-4 over a 3.5 minute period. Each data point represents mean value of $\Delta F/F_0$ from at least 11 recordings per group at a given time. Arrowhead marks the time of Ionomycin addition, which permeabilizes the membrane and acts as a positive control. (D) Western blot of DIV14 cortical neurons treated with bicuculine for specified times. Bar denotes GDE2. Graph quantifying GDE2 protein levels show no change in expression after stimulation. 1 way ANOVA ns p = 0.4692, n = 3 for each timepoint.

Figure S5

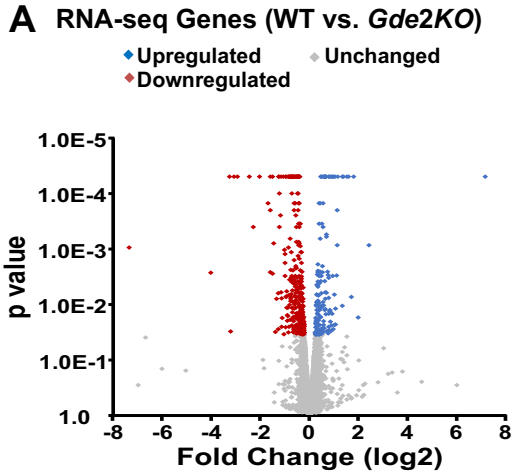

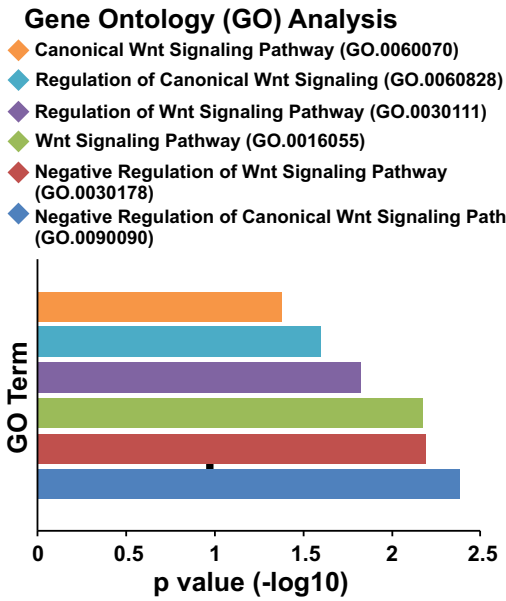

C

Gene name	log2(FC)	p value
Mitf	-2.03989	0.00005
Pttg1	-0.685154	0.00005
Sox9	-0.440899	0.00005
Vegfc	-0.678135	0.00245
Islr	-0.387588	0.0037
Axin2	-0.353966	0.024
Cd44	-0.314482	0.0263

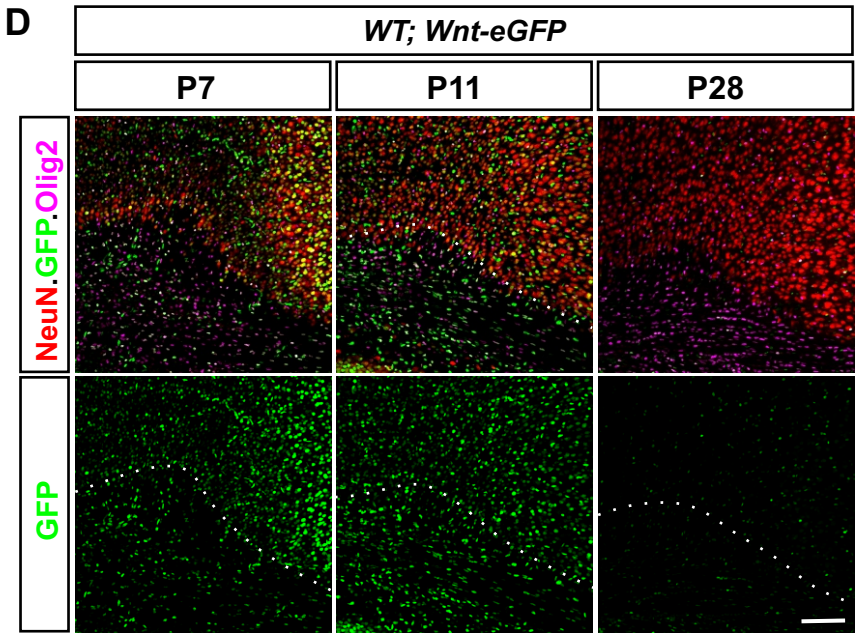

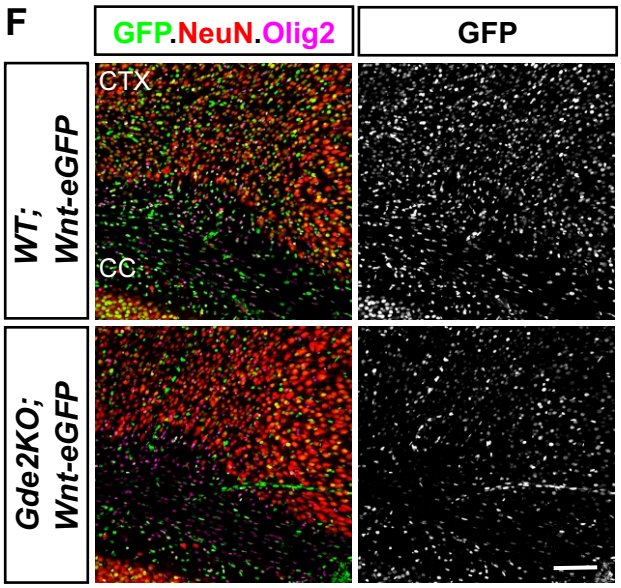

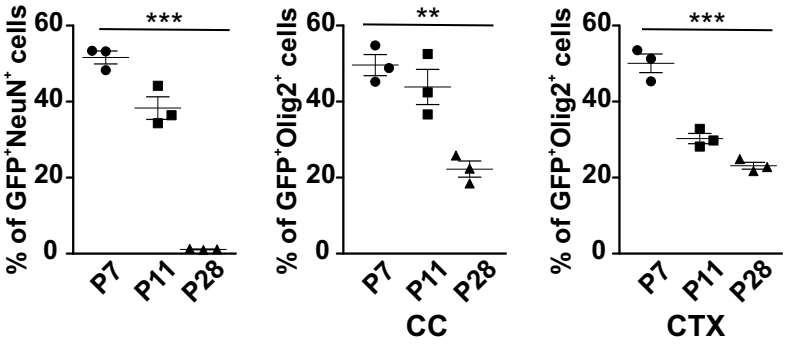

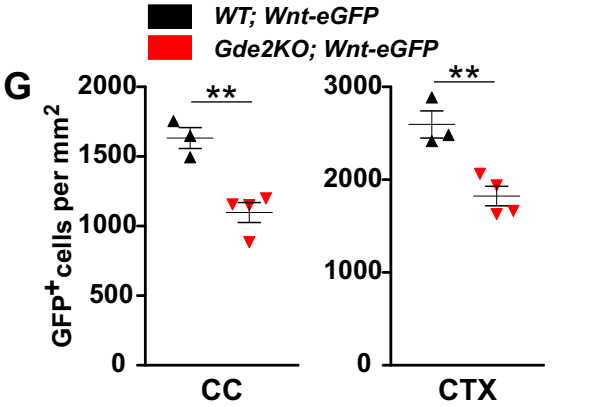

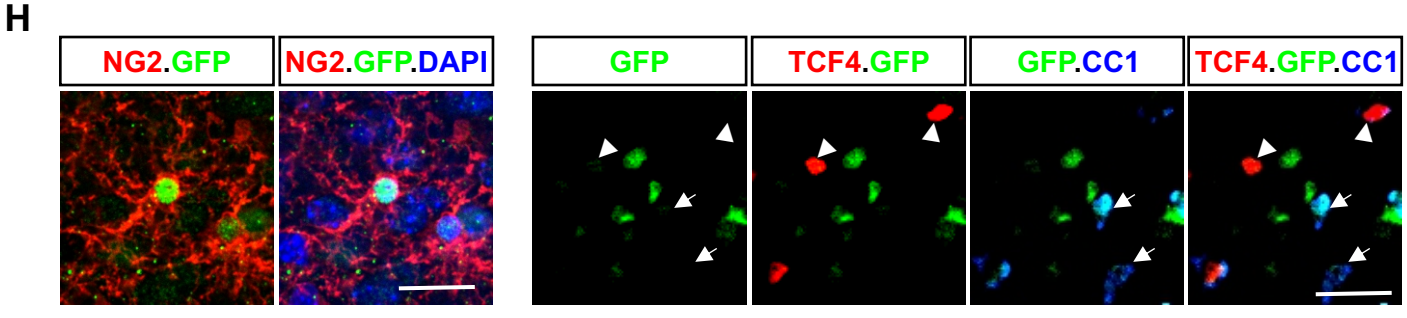

Figure S5. Related to Figure 5. Canonical Wnt signaling is reduced when GDE2 is disrupted. (A) Volcano plot showing differentially expressed genes between WT and *Gde2KO* spinal cord. (B) Gene ontology analysis using p-value (< 0.05) highlights Wnt signaling pathways are disrupted in absence of GDE2. (C) List of known Wnt target genes that are altered in *Gde2KO* condition. (D) Analysis of Wnt-reporter animals (*Wnt-eGFP*) show that canonical Wnt signaling (eGFP) is high at P7 and P11 but is minimal at P28. Hatched line marks the boundary between cortex and corpus callosum. (E) Graphs quantifying the percentage of reporter gene expression in *Wnt-eGFP* mice at P7, P11 and P28 in neurons (NeuN+) and oligodendroglia (Olig2+) in corpus callosum (CC) and cortex (CTX). GFP+NeuN+ ***p < 0.0001, GFP+Olig2+ CC **p = 0.0027, GFP+Olig2+ CTX ***p <0.0001. n = 3 P7, 3 P11, 3 P28, 1-way ANOVA. Data for P11 are the same as presented in Figure 4F and 4H (WT) and are included here for comparison purposes. (F) Coronal sections of P11 *WT; Wnt-eGFP* and *Gde2KO;Wnt-eGFP* animals (G) Graphs quantifying GFP+ cells in CC and CTX. CC **p = 0.004, CTX **p = 0.007, n = 3 *WT; Wnt-eGFP*, 4 *Gde2KO;Wnt-eGFP*, two-tailed unpaired t-test. (H) Representative image of P11 cortex of *Wnt-eGFP* mice. Arrowheads mark TCF4+CC1- immature OLs, arrows mark mature CC1+ OLs; both populations do not co-express eGFP. All graphs: Mean $\pm$ sem. Scale bar: (D, F) 100 μm, (H) 20μm.

Figure S6

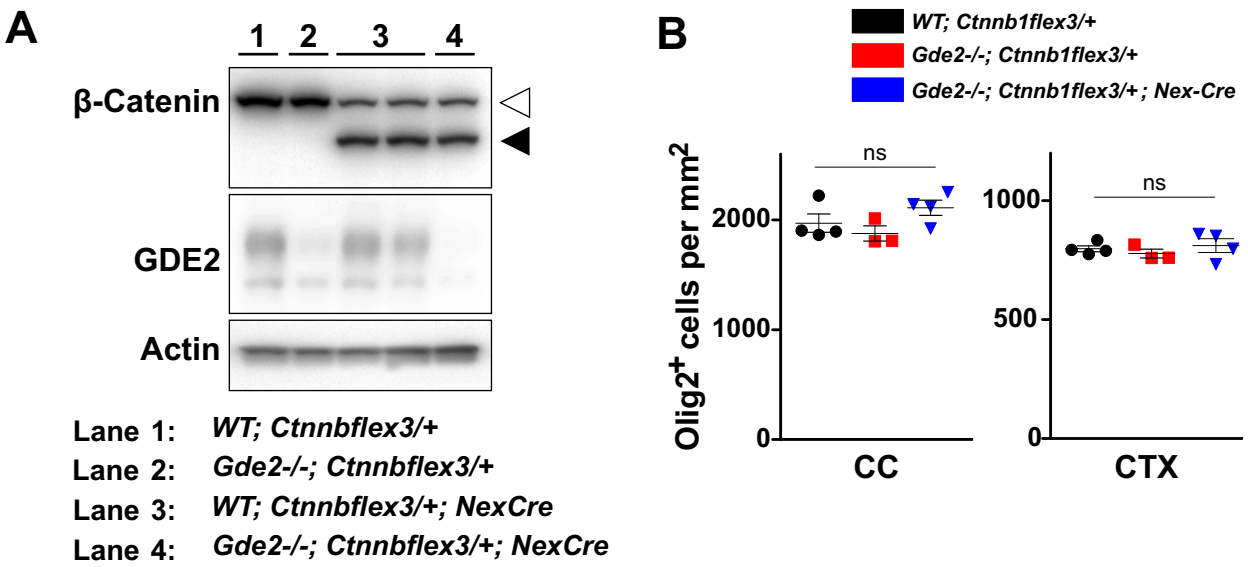
A
1 2 3 4
β-Catenin
GDE2
Actin
Lane 1: WT; Ctnnbflex3/+
Lane 2: Gde2-/-; Ctnnbflex3/+
Lane 3: WT; Ctnnbflex3/+; NexCre
Lane 4: Gde2-/-; Ctnnbflex3/+; NexCre
B
WT; Ctnnb1flex3/+
Gde2-/-; Ctnnb1flex3/+
Gde2-/-; Ctnnb1flex3/+ ; Nex-Cre
Olig2+ cells per mm2
2000
1000
0
ns
CC
1000
500
0
ns
CTX

Figure S6. Related to Figure 6. Genetic stabilization of β-catenin in neurons does not change total Olig2+ cells.

(A) Western blot of P14 cortical extracts. Open arrowhead marks WT β-catenin; black arrowhead marks β-catenin deleted for exon 3. Actin is used as a loading control. (B) Graphs quantifying the number of Olig2+ cells in P11 corpus callosum (CC) and cortex (CTX). ns CC p = 0.1608 (1-way ANOVA/Bonferroni's multiple comparison test), ns CTX p = 0.6109 (1-way ANOVA/Bonferroni's multiple comparison test). n = 4 *WT;β-cat*^{ex3}, 3 *Gde2KO;β-cat*^{ex3}; 4 *Gde2KO;*N-*β-cat*^{ex3}*.* All graphs: Mean ± sem.

Figure S7

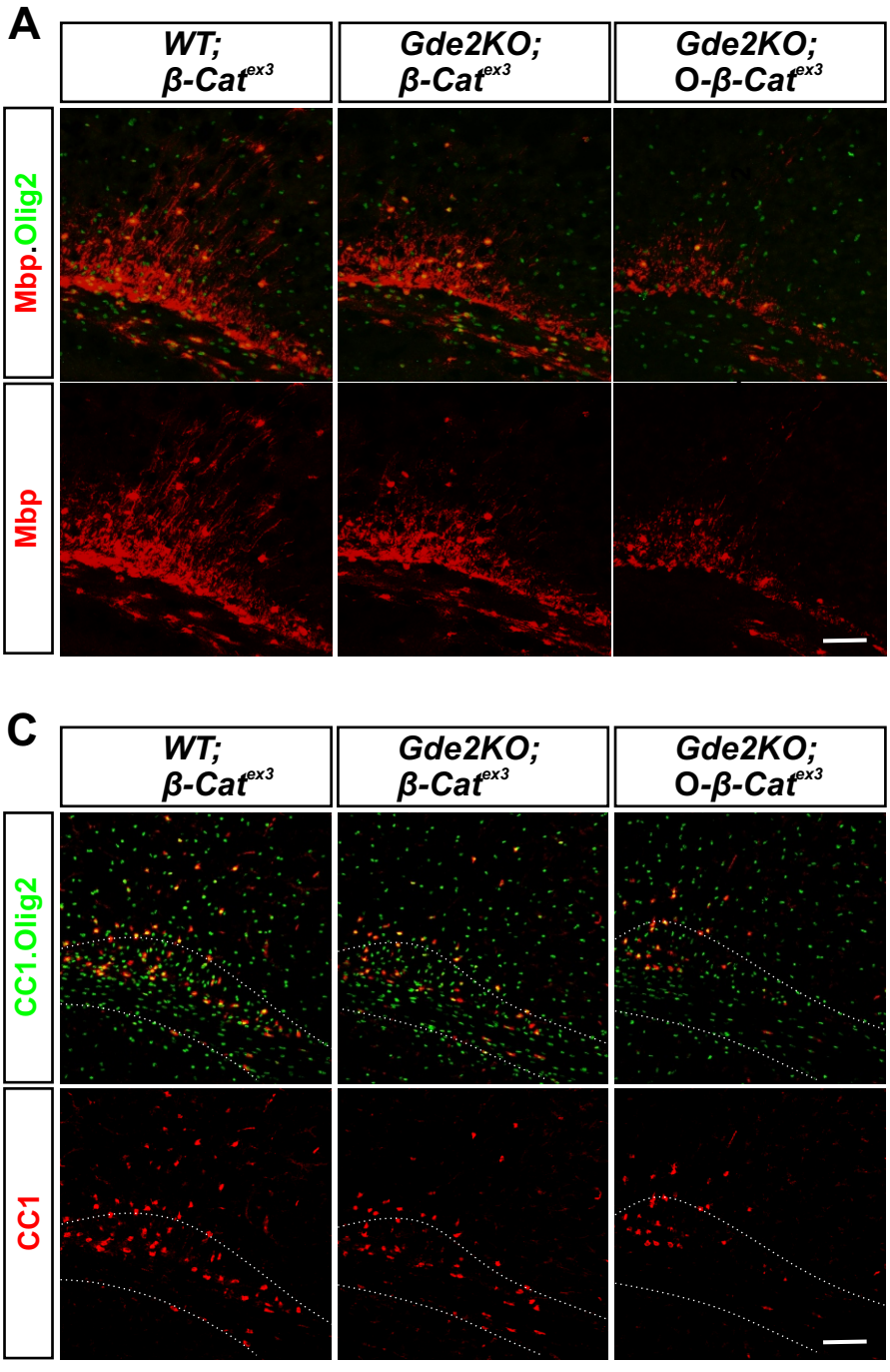
A
WT; β-Cat^ex3
Gde2KO; β-Cat^ex3
Gde2KO; O-β-Cat^ex3
Mbp.Olig2
Mbp
C
WT; β-Cat^ex3
Gde2KO; β-Cat^ex3
Gde2KO; O-β-Cat^ex3
CC1.Olig2
CC1

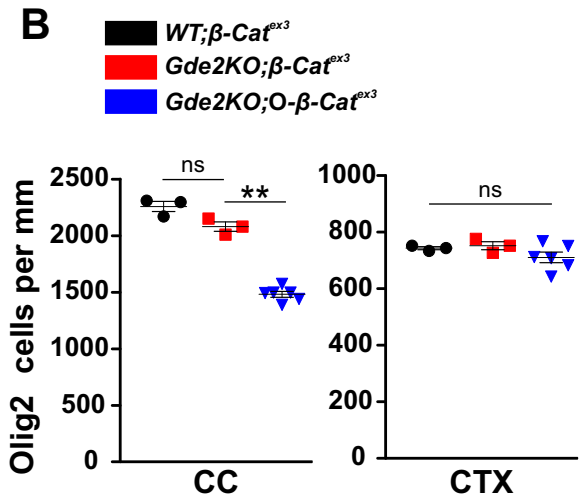
B
WT;β-Cat^ex3
Gde2KO;β-Cat^ex3
Gde2KO;O-β-Cat^ex3
Olig2 cells per mm
2500
2000
1500
1000
500
0
ns
**
CC
1000
800
600
400
200
0
ns
CTX

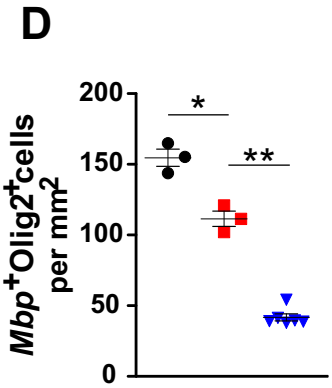
D
Mbp+Olig2+cells per mm2
200
150
100
50
0
*
**

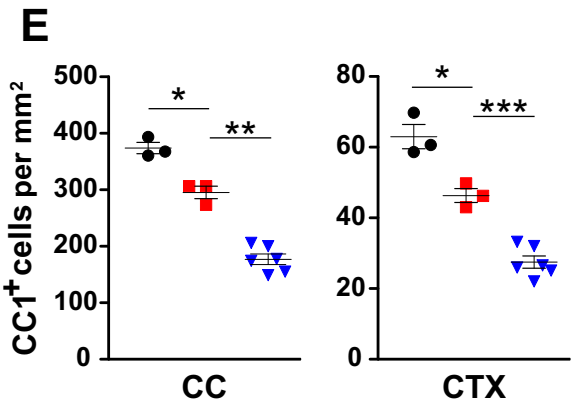
E
CC1+cells per mm2
500
400
300
200
100
0
*
**
CC
80
60
40
20
0
*
***
CTX

Figure S7. Related to Figure 5. Stabilization of β-catenin in OPCs does not rescue *Gde2KO* OL maturation.

(A, C) Coronal sections of P11 mouse cortex (CTX) and corpus callosum (CC). Hatched lines in panel C outlines CC boundaries. (B) Graphs quantifying the number of Olig2+ cells in CC and CTX. CC ns p = 0.0601, **p = 0.0011, two-tailed unpaired t- test; CTX ns p = 0.1235, 1-way ANOVA Bonferroni's multiple comparison test, all 3 genotypes. n = 3 *WT;β-cat^{ex3}*, 3 *Gde2KO;β-cat^{ex3}*, 6 *Gde2KO;*O*-β-cat^{ex3}*. (D) Graph quantifying the number of MBP+Olig2+ cells *p = 0.0132, **p = 0.0073, n = 3 *WT;β-cat^{ex3}*, 3 *Gde2KO;β-cat^{ex3}*, 6 *Gde2KO;*O*-β-cat^{ex3}*. Two tailed unpaired Student's t-test. (E) Graphs quantifying number of CC1+ OLs. CC *p = 0.0132, **p = 0.0012; CTX *p = 0.0242, ***p = 0.0008, n = 3 *WT;β-cat^{ex3}*, 3 *Gde2KO;β-cat^{ex3}*, 6 *Gde2KO;*O*-β-cat^{ex3}*. Two tailed unpaired Student's t-test. All graphs: Mean ± sem. Scale bars: 100 μm.

Figure S8

A

Protein name	Gene name	KO/WT ratio
Glypican-1;Secreted glypican-1	*Gpc1*	0.82
Glypican-2;Secreted glypican-2	*Gpc2*	0.91
Semaphorin-7A	*Sema7a*	0.94
Cadherin-13	*Cdh13*	0.95
Contactin-2 (a.k.a. TAG-1)	*Cntn2*	1.05
Neural cell adhesion molecule 1	*Ncam1*	1.11
RGM domain family member B	*Rgmb*	1.22
Lipoprotein lipase	*Lpl*	1.23
Repulsive guidance molecule A	*Rgma*	1.25
Contactin-1	*Cntn1*	1.25
Neural cell adhesion molecule 2	*Ncam2*	1.40

B

Protein name	*Gene name*	KO/WT ratio
Carboxypeptidase B2	*Cpb2*	0.33
Phosphatidylethanolamine-binding protein 1	*Pebp1*	0.43
Receptor-type tyrosine-protein phosphatase zeta	*Ptprz1*	0.44
Gamma-glutamyl hydrolase	*Ggh*	0.47
Follistatin-related protein 5	*Fstl5*	0.50
Glucose-6-phosphate isomerase	*Gpi*	0.51
ProSAAS	*Pcsk1n*	0.53
Noelin	*Olfm1*	0.53
Glia-derived nexin	*Serpine2*	0.54
Complement C5	*C5*	0.57
Collagen alpha-1(I) chain	*Col1a1*	3.98

C

1 CM
2 CM Phosphacan depleted

D

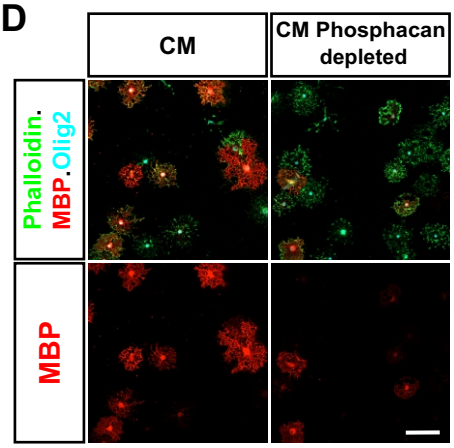

E

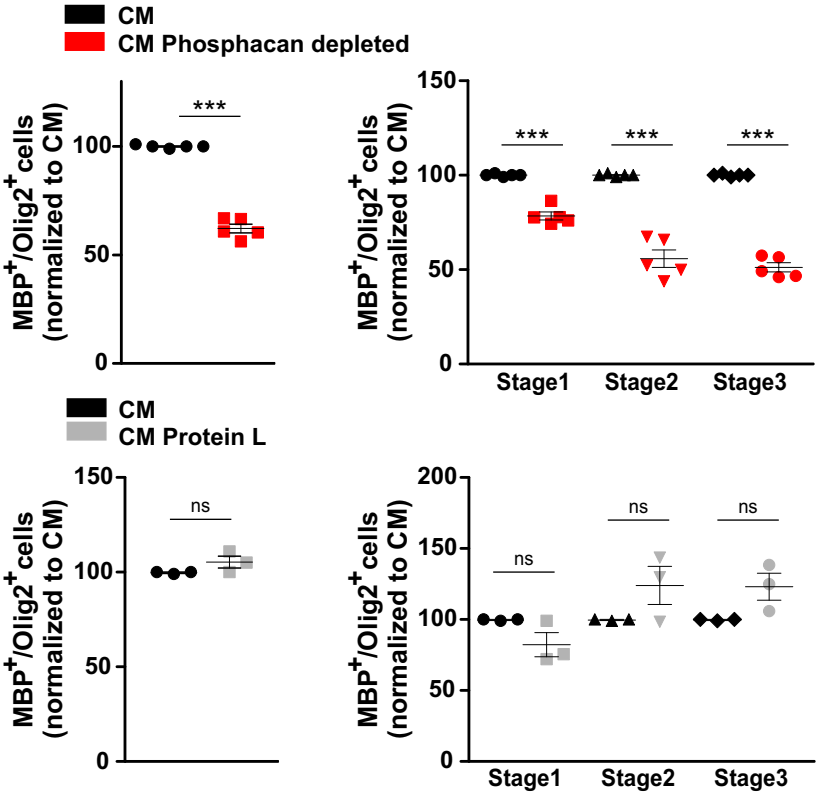

F

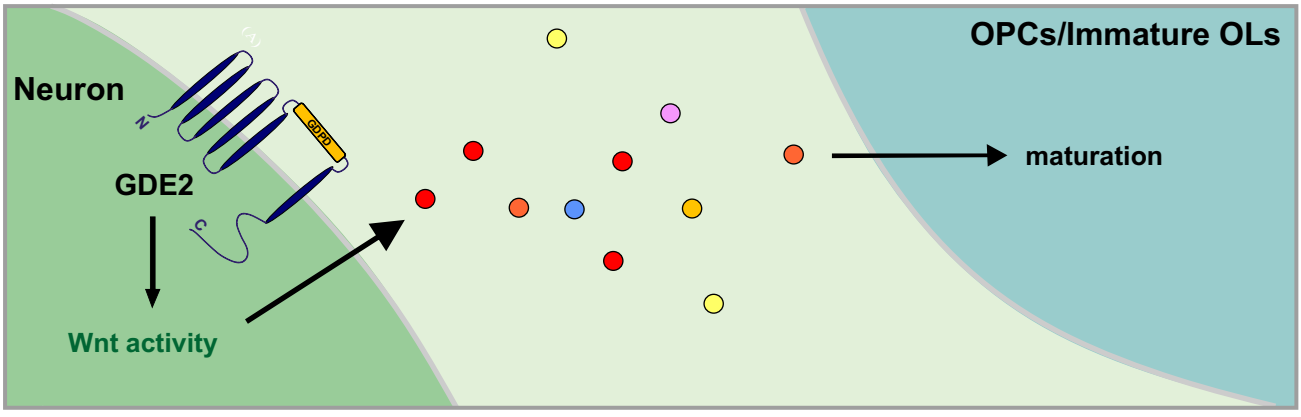

Figure S8. Related to Figure 7. Candidate mechanisms for GDE2-dependent OL maturation. (A) List of GPI-anchored proteins identified in WT and *Gde2KO* CM by mass spectrometry. (B) List of secreted and extracellular matrix proteins identified in WT and *Gde2KO* CM by mass spectrometry. RPTPzeta (phosphacan) is highlighted in red. (C) Western blot of WT neuronal CM showing effective depletion of phosphacan using neuronal phosphacan antibodies conjugated to protein-L (D) Representative images of WT OPCs after culturing with WT neuronal CM and WT neuronal CM depleted for phosphacan. (E) Graphs quantifying the percentage of MBP+Olig2+ OLs (normalized to WT CM) in WT OPC cultures grown with WT neuronal CM or phosphacan depleted WT neuronal CM. Top panel ***p<0.0001, n = 5 WT CM, 5 Phosphacan depleted CM, two tailed unpaired t-test. All 3 stages of OL maturation are also affected (2-way ANOVA ***p < 0.0001; Bonferroni correction Stage 1 ***p <0.001; Stage 2 ***p <0.001; Stage 3 ***p <0.001; n = 5 WT CM, 5 Phosphacan depleted CM. No change in OPC maturation is observed between WT neuronal CM or WT neuronal CM preincubated with protein L alone. Bottom panel ns p = 0.1456, n = 3 WT CM, 3 Protein L incubated CM, two tailed unpaired t-test. Similarly, stages of OL maturation are unchanged (2-way ANOVA ns p = 0.1262; Bonferroni correction Stage 1 ns p >0.05; Stage 2 ns p >0.05; Stage 3 ns p >0.05; n = 5 WT CM, 5 Phosphacan depleted CM.(F) Model for GDE2 regulation of OL maturation. GDE2 stimulates canonical Wnt signaling in neurons. Wnt activation leads to release of neuronally-derived factors such as phosphacan, which act on neighboring OPCs or immature OLs to promote their maturation into myelinating oligodendrocytes.

Table S1: Cell counts for in vitro cultures. Refers to Figure 4, Figure 7, and Figure S8.

Fig 4

B/F			D/F			D		
DIV3+4_coculture	WT	*Gde2KO*	DIV3+4 CM	WT	*Gde2KO*	DIV3 CM	WT	*Gde2KO*
Olig2+	2959	3030	Olig2+	1251	1126	Olig2+	730	907
MBP_stage 1	159	89	MBP_stage 1	251	194	MBP_stage 1	50	60
MBP_stage 2	116	43	MBP_stage 2	219	147	MBP_stage 2	71	51
MBP_Stage 3	53	18	MBP_Stage 3	62	30	MBP_Stage 3	48	27
total MBP+	328	152	total MBP+	532	371	total MBP+	169	138

Fig 7B

	Gde2KO;β-Cat^{ex3} CM	*Gde2KO;* N-*β-Cat*^{ex3} CM
Olig2+	936	894
MBP_stage 1	65	100
MBP_stage 2	26	43
MBP_Stage 3	17	28
total MBP+	108	171

Fig S8E

	CM	CM phsophacan depleted		CM	CM protein L
Olig2+	2189	2815	Olig2+	1007	869
MBP_stage 1	290	306	MBP_stage 1	132	97
MBP_stage 2	377	278	MBP_stage 2	132	140
MBP_Stage 3	189	138	MBP_Stage 3	61	67
total MBP+	856	722	total MBP+	325	304

Table S3: Related to Supplemental Figure 8. List of proteins showing > 40% differential enrichment in *Gde2KO* CM.

Number of altered protein expression: 149

Protein IDs	Protein names	Gene names	Sequence coverage KO [%]	Sequence coverage WT [%]	LFQ intensity KO	LFQ intensity WT	Ratio (KO/WT)
A8DUK4	beta-globin	*Hbbt1*	60.9	58.2	3.67E+06	3.93E+08	0.0093385
Q80ZV4	Cadherin-4	*Cdh4*	3.6	3.6	3.59E+05	6.73E+06	0.0533103
P35979	60S ribosomal protein L12	*Olfm1*	9.7	9.7	3.50E+05	3.35E+06	0.104707
Q3TLP8	Ras-related C3 botulinum toxin substrate 1	*Rac1*	9.45	12.3	1.22E+06	1.16E+07	0.1055619
P58283	E3 ubiquitin-protein ligase RNF216	*Rnf216*	0.8	0.8	7.20E+05	5.81E+06	0.1241085
Q6ZWQ9	Myosin regulatory light chain 12B	*Myl12a*	17.4	9.3	2.92E+06	2.11E+07	0.1384735
P48678	Prelamin-A/C	*Lmna*	1.8	0.75	7.71E+04	3.94E+05	0.1955637
F6VYE2	Zinc finger MYM-type protein 4	*Zmym4*	0.7	0.7	3.81E+07	1.28E+08	0.2985482
G5E866	Splicing factor 3B subunit 1	*Sf3b1*	0.35	1.1	6.29E+05	2.08E+06	0.3018324
Q99JI6	Ras-related protein Rap-1b	*Rap1b*	11.15	11.15	2.20E+06	7.24E+06	0.304105
P62897	Cytochrome c, somatic	*Cycs*	17.15	17.15	1.47E+06	4.78E+06	0.3074461
P32233	Developmentally-regulated GTP-binding protein 1	*Drg1*	4.4	4.4	4.55E+05	1.37E+06	0.3315903
Q2KIG3	Carboxypeptidase B2	*Cpb2*	2.6	2.15	2.81E+05	8.34E+05	0.3367496
P19253	60S ribosomal protein L13a	*Rpl13a*	8.1	8.1	1.20E+06	3.52E+06	0.3409558
P97350	Plakophilin-1	*Pkp1*	2.25	2.25	2.43E+06	6.66E+06	0.3647232
P62242	40S ribosomal protein S8	*Rps8*	8.9	7.2	7.11E+05	1.75E+06	0.4058655
Q3UHN9	Bifunctional heparan sulfate N-deacetylase	*Ndst1*	0.8	1.6	9.53E+05	2.35E+06	0.4063519
A0A087WPL5	ATP-dependent RNA helicase A	*Dhx9*	0.6	0.85	4.55E+05	1.11E+06	0.4094201
Q8QZY9	Splicing factor 3B subunit 4	*Sf3b4*	1.65	3.3	2.16E+06	5.03E+06	0.4288
P70296	Phosphatidylethanolamine-binding protein 1	*Pebp1*	32.6	29.15	4.56E+07	1.05E+08	0.4363098
Q62189	U1 small nuclear ribonucleoprotein A	*Snrpa*	9.55	9.55	7.22E+06	1.64E+07	0.4395122
B9EKR1	Receptor-type tyrosine-protein phosphatase zeta	*Ptprz1*	7.05	6.8	1.08E+08	2.43E+08	0.445375
Q9DBG3	AP-2 complex subunit beta;AP complex subunit beta	*Ap2b1*	2	1.3	2.06E+06	4.55E+06	0.4524362
Q60648	Ganglioside GM2 activator	*Gm2a*	8.8	4.4	1.39E+06	2.98E+06	0.4666868
Q9CXV9	DCN1-like protein 5	*Dcun1d5*	6.3	6.3	3.76E+07	8.06E+07	0.466781
Q9Z0L8	Gamma-glutamyl hydrolase	*Ggh*	12.9	12.9	6.49E+06	1.37E+07	0.4751144
P80317	T-complex protein 1 subunit zeta	*Cct6a*	4.35	2.85	1.13E+06	2.35E+06	0.4792104
B1AX58	Plastin-3	*Pls3*	0.7	1.4	8.46E+05	1.76E+06	0.4811927
Q9R1P3	Proteasome subunit beta type-2	*Psmb2*	6.2	9.95	8.15E+06	1.65E+07	0.4936686
Q8R093	Uridine phosphorylase	*Upp2*	4.2	2.1	5.18E+07	1.03E+08	0.5007006
Q8BFR2	Follistatin-related protein 5	*Fstl5*	8	9.8	1.04E+07	2.08E+07	0.5017444
Q9EST1	Gasdermin-A	*Gsdma*	1	2.6	1.80E+06	3.50E+06	0.5148759
Q91V64	Isochorismatase domain-containing protein 1	*Isoc1*	5.2	10.4	1.33E+06	2.58E+06	0.5164249
P06745	Glucose-6-phosphate isomerase	*Gpi*	5.2	5.2	9.57E+05	1.84E+06	0.518811
Q9CQU0	Thioredoxin domain-containing protein 12	*Txndc12*	6.45	4.4	1.93E+06	3.68E+06	0.5235417
Q08331	Calretinin	*Calb2*	11.8	11.8	3.97E+06	7.51E+06	0.5290136
Q9QXV0	ProSAAS	*Pcsk1n*	12.2	10.5	9.84E+06	1.85E+07	0.53233
A3KGE4	Noelin	*Olfm1*	4.3	4.3	7.73E+05	1.44E+06	0.5356937
Q3TKX1	V-type proton ATPase subunit S1	*Atp6ap1*	14.2	14.2	1.28E+07	2.37E+07	0.5403885
Q9DAY9	Nucleophosmin	*Npm1*	4.1	14	1.17E+07	2.15E+07	0.5426547
Q07235	Glia-derived nexin	*Serpine2*	13.35	13.35	5.49E+06	1.00E+07	0.5480371
Q9JJU8	SH3 domain-binding glutamic acid-rich-like protein	*Sh3bgrl*	25	18	7.48E+06	1.36E+07	0.548844
P61164	Alpha-centractin	*Actr1a*	2.95	7.85	1.46E+06	2.65E+06	0.550069
P61358	60S ribosomal protein L27	*Rpl27*	7.35	10.65	2.31E+06	4.20E+06	0.5504141
O09061	Proteasome subunit beta type-1	*Psmb1*	14.15	18.3	1.62E+07	2.92E+07	0.5534894
Q5RKN9	F-actin-capping protein subunit alpha-1	*Capza1*	13.6	13.6	4.36E+06	7.85E+06	0.5548677
E9PYH2	Cytosolic acyl coenzyme A thioester hydrolase	*Acot7*	8.3	6.75	6.44E+06	1.15E+07	0.559416
P24369	Peptidyl-prolyl cis-trans isomerase B	*Ppib*	18.05	16	2.04E+07	3.62E+07	0.5644408
Q9D1C8	Vacuolar protein sorting-associated protein 28 homolog	*Vps28*	2.75	5.5	7.42E+05	1.31E+06	0.5652669
Q3TX55	Actin-related protein 2/3 complex subunit 4	*Arpc4*	20.25	17.9	1.39E+07	2.44E+07	0.569117
P62702	40S ribosomal protein S4	*Gm15013*	5.1	8.1	7.23E+06	1.27E+07	0.569801
S4R1N6	40S ribosomal protein S18	*Rps18*	22.9	18.7	1.08E+07	1.88E+07	0.5729743
P06684	Complement C5	*C5*	1.05	1.05	2.07E+06	3.60E+06	0.5752787
D3Z6E4	Enolase;Gamma-enolase	*Eno2*	6.35	7.9	4.46E+05	7.64E+05	0.5833966
P50247	Adenosylhomocysteinase	*Ahcy*	9	9	5.44E+06	9.19E+06	0.5925307
P20029	78 kDa glucose-regulated protein	*Hspa5*	7.25	9.4	2.20E+06	3.68E+06	0.5991105
P55821	Stathmin-2	*Stmn2*	14.5	14.5	2.67E+07	1.91E+07	1.4007286
O35136	Neural cell adhesion molecule 2	*Ncam2*	3.5	3.5	2.09E+06	1.49E+06	1.4047028
Q60994	Adiponectin	*Adipoq*	10.75	10.75	7.19E+07	5.10E+07	1.4090303
Q60864	Stress-induced-phosphoprotein 1	*Stip1*	2.9	2.9	5.38E+06	3.81E+06	1.4108147
D3YYE1	Acidic leucine-rich nuclear phosphoprotein 32 family member A	*Anp32a*	13.9	17.2	1.19E+07	8.38E+06	1.4150217
Q8BGQ7	Alanine--tRNA ligase, cytoplasmic	*Aars*	0.9	0.9	1.01E+06	7.09E+05	1.4222222
Q93092	Transaldolase	*Taldo1*	14	11.5	1.43E+08	9.97E+07	1.4302839
Q99J36	THUMP domain-containing protein 1	*Thumpd1*	8.45	7.3	2.46E+06	1.72E+06	1.434379
Q99PT1	Rho GDP-dissociation inhibitor 1	*Arhgdia*	29.9	30.15	8.03E+07	5.58E+07	1.4393366
Q61598	Rab GDP dissociation inhibitor beta	*Gdi2*	17.75	16.95	5.91E+07	4.07E+07	1.4504449
A2A4I8	Amine oxidase	*Aoc3*	1.9	1.9	1.04E+08	7.17E+07	1.45059
P08030	Adenine phosphoribosyltransferase	*Aprt*	10	7.2	4.33E+06	2.98E+06	1.4560516
P21460	Cystatin-C	*Cst3*	27.5	27.5	5.77E+08	3.93E+08	1.4677356
P35441	Thrombospondin-1	*Thbs1*	4.8	5	6.15E+06	4.14E+06	1.4860469
P04444	Hemoglobin subunit beta-H1	*Hbb-bh1*	21.1	21.1	7.56E+06	5.08E+06	1.4896048
P02104	Hemoglobin subunit epsilon-Y2	*Hbb-y*	40.15	39.15	2.39E+08	1.60E+08	1.4902499
Q8CBG6	6-phosphogluconolactonase	*Pgls*	7.2	10.9	4.86E+06	3.26E+06	1.4918735
P63158	High mobility group protein B1	*Hmgb1*	24.3	24	5.03E+07	3.37E+07	1.4921339
Q564E2	L-lactate dehydrogenase	*Ldha*	32.5	32.5	1.43E+08	9.51E+07	1.5027012
P34022	Ran-specific GTPase-activating protein	*Ranbp1*	8.1	10.8	5.39E+06	3.58E+06	1.5047218
P62869	Transcription elongation factor B polypeptide 2	*Tceb2*	26.25	22	7.90E+06	5.24E+06	1.5070908
O70251	Elongation factor 1-beta	*Eef1b2*	11.7	15.2	6.12E+06	4.03E+06	1.5189003
Q9WU60	Attractin	*Atrn*	0.55	0.55	2.72E+06	1.78E+06	1.5249867

A2AI62	Hephaestin	*Heph*	0.9	0.9	6.04E+07	3.94E+07	1.5319845
Q5XJF6	Ribosomal protein	*Rpl10a*	12.4	12.4	1.26E+07	8.16E+06	1.5469304
Q9WTP6	Adenylate kinase 2	*Ak2*	6.9	4.2	6.54E+05	4.19E+05	1.560639
P21619	Lamin-B2	*Lmnb2*	2.3	1.15	8.17E+05	5.23E+05	1.5621844
P10126	Elongation factor 1-alpha 1	*Eef1a1*	15.35	12.75	2.10E+09	1.33E+09	1.5713376
Q5SXR6	Clathrin heavy chain;Clathrin heavy chain 1	*Cltc*	10.55	10.15	6.69E+07	4.26E+07	1.5719838
Q9CQI6	Coactosin-like protein	*Cotl1*	14.45	16.55	1.03E+08	6.50E+07	1.5812476
Q6P1J1	Dihydropyrimidinase-related protein 1	*Crmp1*	6.15	6.15	5.37E+06	3.38E+06	1.5860785
B2M1R7	Poly(rC)-binding protein 2	*Pcbp2*	14.25	13.85	1.76E+07	1.11E+07	1.5870965
Q9DCD0	6-phosphogluconate dehydrogenase, decarboxylating	*Pgd*	5.8	5.8	1.23E+07	7.69E+06	1.6018917
Q8BHZ0	Protein FAM49A	*Fam49a*	8.5	6.5	7.84E+05	4.87E+05	1.6099238
P35585	AP-1 complex subunit mu-1	*Ap1m1*	5.8	4.05	1.90E+06	1.17E+06	1.627294
Q61171	Peroxiredoxin-2	*Prdx2*	25	25	5.06E+08	3.10E+08	1.6326191
F6ZBL2	E3 ubiquitin-protein ligase MIB1	*Mib1*	2.5	2.5	1.95E+09	1.18E+09	1.6437232
Q3U3V1	Coagulation factor X	*F10*	1.8	1.8	3.78E+06	2.28E+06	1.6583261
Q8BTU6	Eukaryotic initiation factor 4A-II	*Eif4a2*	24.2	21.65	9.47E+06	5.57E+06	1.6980858
P43277	Histone H1.3	*Hist1h1d*	18.55	18.55	2.84E+08	1.67E+08	1.6982031
Q91WU0	Carboxylic ester hydrolase	*Ces1f*	2.1	2.1	6.60E+07	3.84E+07	1.7195086
E0CZ27	Histone H3	*H3f3a*	15.55	19.3	5.70E+08	3.30E+08	1.7248706
E9Q6B6	C-Jun-amino-terminal kinase-interacting protein 3	*Mapk8ip3*	1.4	1.4	3.23E+07	1.86E+07	1.7333405
Q8BIZ0	Protocadherin-20	*Pcdh20*	0.7	0.7	6.59E+05	3.79E+05	1.7368837
P29788	Vitronectin	*Vtn*	3.8	3.8	2.38E+06	1.35E+06	1.7573225
Q9CQV8	14-3-3 protein beta/alpha	*Ywhab*	20.9	23.15	4.20E+07	2.38E+07	1.7635641
P17897	Lysozyme C-1	*Lyz1*	8.1	8.1	3.90E+06	2.19E+06	1.7755069
P97333	Neuropilin-1	*Nrp1*	2.3	3.1	3.55E+06	1.99E+06	1.7817533
G3X9I4	Aly/REF export factor 2	*Alyref2*	5	5	1.75E+07	9.73E+06	1.8022802
P63260	Actin	*Actg1*	47.6	44.65	3.53E+06	1.94E+06	1.8262027
P62082	40S ribosomal protein S7	*Rps7*	2.1	2.1	7.19E+06	3.94E+06	1.8266545
H7BX52	Cullin-2	*Cul2*	17.8	17.8	5.21E+06	2.85E+06	1.8277042
Q9R1P1	Proteasome subunit beta type-3	*Psmb3*	6.8	3.4	6.64E+06	3.63E+06	1.8284916
F6W8R9	Nesprin-2	*Syne2*	1.1	0.55	7.38E+06	4.00E+06	1.843401
Q8VEK3	Heterogeneous nuclear ribonucleoprotein U	*Hnrnpu*	4.65	4.65	5.36E+06	2.89E+06	1.8557495
A2A813	Protein deglycase DJ-1	*Park7*	9.1	7.7	7.71E+06	4.15E+06	1.8572581
G3UZR0	N(G),N(G)-dimethylarginine dimethylaminohydrolase 2	*Ddah2*	16.55	19.7	3.48E+06	1.87E+06	1.8595037
P2604	Moesin	*Msn*	4.75	4.75	3.57E+06	1.91E+06	1.8641588
Q9JMG7	Hepatoma-derived growth factor-related protein 3	*Hdgfrp3*	8.2	8.2	2.53E+06	1.34E+06	1.8807877
D3Z7E6	Platelet-activating factor acetylhydrolase IB subunit gamma	*Pafah1b3*	13.9	16.4	8.71E+06	4.61E+06	1.8873094
Q5SW88	Ras-related protein Rab-1A	*Rab1*	8.9	12.4	1.80E+07	9.38E+06	1.9214568
Q61233	Plastin-2	*Lcp1*	9	6.45	1.52E+07	7.75E+06	1.9644182
D3Z315	Coatomer subunit epsilon	*Cope*	7.3	9.9	1.54E+06	7.76E+05	1.9872323
P26645	Myristoylated alanine-rich C-kinase substrate	*Marcks*	16.2	8.1	5.31E+06	2.52E+06	2.1103271
Q62084	Protein phosphatase 1 regulatory subunit 14B	*Ppp1r14b*	17	17.35	8.34E+06	3.89E+06	2.1448012
G3UY42	Polyadenylate-binding protein 2	*Pabpn1*	8.5	8.5	2.45E+06	1.12E+06	2.1813408
B7FAV1	Filamin-A	*Flna*	1	0.3	2.64E+06	1.19E+06	2.217373
Q9CQI3	Glia maturation factor beta	*Gmfb*	14.6	14.6	1.14E+07	5.01E+06	2.267461
H7BXC3	Triosephosphate isomerase	*Tpi1*	12.9	12.6	4.71E+06	2.07E+06	2.2687512
Q60865	Caprin-1	*Caprin1*	3.3	3.3	2.74E+07	1.20E+07	2.2891093
F6Q2E3	26S protease regulatory subunit 6A	*Psmc3*	7.9	3.95	6.35E+05	2.72E+05	2.3318521
F6VRI6	Ubiquitin-like modifier-activating enzyme 5	*Uba5*	16.2	8.1	5.56E+05	2.33E+05	2.383202
P60867	40S ribosomal protein S20	*Rps20*	14.25	9.65	1.46E+07	6.10E+06	2.3875143
Q14AA6	GTP-binding nuclear protein Ran	*Ran*	9.7	14.8	5.11E+07	2.13E+07	2.3989767
P68134	Actin, alpha skeletal muscle	*Acta1*	26.4	23.45	8.55E+07	3.55E+07	2.4108667
P35700	Peroxiredoxin-1	*Prdx1*	17.75	20.15	6.77E+07	2.75E+07	2.4657958
P02089	Hemoglobin subunit beta-2	*Hbb-b2*	46.9	46.6	1.84E+08	7.40E+07	2.4912119
Q04750	DNA topoisomerase 1	*Top1*	2.1	2.1	1.98E+06	7.37E+05	2.6873618
Q543K9	Purine nucleoside phosphorylase	*Pnp;Pnp2*	6.6	3.3	7.72E+05	2.84E+05	2.7204358
Q8CGP4	Histone H2A	*Hist1h2aa*	21.4	21.4	4.88E+08	1.74E+08	2.8048444
P83917	Chromobox protein homolog 1	*Cbx1*	9.2	7.55	1.22E+06	4.26E+05	2.8537753
O35864	COP9 signalosome complex subunit 5	*Cops5*	14.3	14.3	4.69E+06	1.63E+06	2.8804678
Q9CR00	26S proteasome non-ATPase regulatory subunit 9	*Psmd9*	5.1	2.55	4.20E+06	1.36E+06	3.0804593
P00015	Cytochrome c, testis-specific	*Cyct*	24.3	17.65	1.89E+07	5.88E+06	3.2051827
P28658	Ataxin-10	*Atxn10*	1.45	1.45	8.12E+05	2.29E+05	3.5437179
P20357	Microtubule-associated protein 2	*Map2*	1.75	1.4	4.00E+06	1.13E+06	3.5489953
P61750	ADP-ribosylation factor 4	*Arf4*	11.7	11.7	9.87E+06	2.49E+06	3.955426
P11087	Collagen alpha-1(I) chain	*Col1a1*	6.15	3.95	1.68E+07	4.21E+06	3.9850303
P97379	Ras GTPase-activating protein-binding protein 2	*G3bp2*	12	12	3.87E+06	9.04E+05	4.278474
D3Z7K0	Ubiquitin thioesterase OTUB1	*Otub1*	18.65	14.9	2.72E+07	5.13E+06	5.3105051
P27048	Small nuclear ribonucleoprotein-associated protein B	*Snrpb*	8.25	3.25	1.68E+06	2.01E+05	8.3721104
P35396	Peroxisome proliferator-activated receptor delta	*Ppard*	1.6	1.6	1.39E+08	1.00E+07	13.877689
P07309	Transthyretin	*Ttr*	11.9	5.1	7.35E+07	1.55E+06	47.408315